FIRST ANNUAL REPORT

NASA Research Grant NAG 8-724

Period of Performance
7/1/88 through 6/30/89

VIBRATION ISOLATION TECHNOLOGY: SENSITIVITY OF SELECTED CLASSES OF SPACE EXPERIMENTS TO RESIDUAL ACCELERATIONS

J. IWAN D. ALEXANDER
(Principal Investigator)

Y. Q ZHANG

and

ADEBIMPE ADEBIYI

Center for Microgravity and Materials Research
The University of Alabama in Huntsville
Huntsville, Alabama 35899

TABLE OF CONTENTS

VIBRATION ISOLATION TECHNOLOGY: SENSITIVITY OF SELECTED CLASSES OF SPACE EXPERIMENTS TO RESIDUAL ACCELERATIONS

1. Introduction

The work performed during the first annual period (7/1/88 - 6/30/89) under Grant NAG8-724 involves tasks 1-4 defined in Appendix A. Progress on each task is described in the following sections. Section 2 deals with order of magnitude analyses related to liquid zone sensitivity and thermo-capillary flow sensitivity. Section 3 describes our progress with numerical models of the sensitivity of isothermal liquid zones. Progress towards a numerical model of coupled buoyancy-driven and thermo-capillary convection experiments is described in section 4. Section 5 describes interaction with NASA personnel. Section 6 summarizes our results to date and discusses them in terms of the predicted space station acceleration environment. Work planned for the second year is also discussed in section 6.

2. Order of magnitude estimates[1]

2.1 Introduction

An order of magnitude (OM) or dimensional analysis of a physical process involves the examination of the system of equations that are assumed to govern the process. As far as the candidate experiments for vibration isolation are concerned, the relevant physical processes are governed by equations describing the transport of heat, mass and momentum in single and multi-component fluid systems. The usual approach to OM analyses [1] involves the definition of reference quantities which appropriately characterize the physical system (i.e. reference scales for velocity, time, length, forces, etc.). Application of these scales to the (dimensional) governing equations, followed by the

[1]A description of order of magnitude estimates pertinent to Vibration Isolation Technology was presented by the P.I. at the Vibration Isolation Technology Workshop, Cleveland, 9/28-29/88. As requested by the chairman of the workshop, J. Lubomski (NASA/LeRC), the P. I. submitted a written summary of this presentation to be included in the workshop proceedings. In addition a publication reviewing work related to the effects of oscillating body forces on fluids, and estimates of residual acceleration effects is close to completion .

definition of characteristic dimensionless groups admits a comparison of the order of magnitudes of every term in each equation. There are several comprehensive discussions of OM analyses applied to low gravity situations (eg. [1-4]).

The most extensive treatment of experiment sensitivity to date involves OM estimates [2]. The advantage of this approach is that a great deal of information pertaining to the sensitivity of a given experiment can be obtained without much computational effort. The disadvantages are related to the fact that the choice of characteristic reference quantities for length, velocity, time etc. are not, in general, known *a priori*. Thus, in cases for which the chosen characteristic scale is not (for a given set of conditions) representative of the actual process, the results of the analysis may be in error, often by several orders of magnitude. In addition, application of order of magnitude analyses to the problem of *g-sensitivity* has invariably involved implicit linearization which can also lead to incorrect OM predictions. Finally, analyses are generally restricted to the examination of a single component disturbance (e.g. ~ cos(ωt)). As a result, they may not properly indicate the response of the system to the typically complex multi-frequency disturbances characteristic of the spacecraft environment.

It is, nonetheless, useful to examine the general trends predicted by such analyses since they can provide at least qualitative guidance for more detailed analytical and numerical studies.

The determination of tolerable g-levels using OM analyses is based upon estimates of the response of the system either to steady accelerations, or to time dependent accelerations of the form

$$\mathbf{g}(t) = \mathbf{a}\cos(\omega t) \tag{2.1}$$

where ω is the angular frequency of the disturbance. The susceptibility of an experimental system to such disturbances is defined via the magnitude of a particular response (say a temperature, compositional or velocity fluctuation) which must not be exceeded in order to bring the experiment to a successful conclusion. The most obvious trend predicted by analyses to date are shown in Figs. 1 - 3. The curves depict the maximum tolerable magnitude of a residual acceleration with a given frequency, $\nu = \omega/2\pi$, for a particular experiment and have the form

$$g_{max} = F(\omega, \Pi_{crit}, p_i) \tag{2.2}$$

where Π_{crit} is the magnitude of the maximum allowable response, and the p_i (i=1,N) represent the N material and geometric properties of the system (such as viscosity, thermal and solute diffusivities). Below 10^{-2} to 10^{-3} Hz the response is not dependent (or weakly dependent) on frequency. At frequencies between 10^{-2} and 1 Hz the analyses indicate that the allowable residual acceleration magnitude increases as the frequency is increased. At higher frequencies the allowable magnitude varies inversely with the frequency. This behavior can be understood upon consideration of the following OM estimates [2] (used to obtain Fig. 1) for velocity, temperature and concentration changes associated with the disturbance (2.1):

$$V \sim \frac{g\Delta\rho/\rho}{(\omega^2 + \nu^2/L^4)^{1/2}} \tag{2.3}$$

$$\delta T \sim \frac{g\Delta\rho/\rho}{(\omega^2 + \kappa^2/L^4)^{1/2}} \tag{2.4}$$

$$\delta C \sim \frac{g\Delta\rho/\rho}{(\omega^2 + D^2/L^4)^{1/2}} \tag{2.5}$$

where ν, κ and D are, respectively, diffusivities for momentum, heat and concentration. The sensitivity limits are obtained by using either δT, δC or V as a sensitivity parameter and taking $g = g_{max}$, where g_{max} is the allowable residual acceleration.

In reality, microgravity disturbances tend to be associated with more than one frequency. Given that a system may respond to a multi-frequency disturbance in an "additive" way, tolerance curves such as Figs. 1-3 may underestimate the response to a given microgravity disturbance. For example, models of the DMOS experiment, which flew on STS-61-B, show that mass transport has an additive response to the (multi-frequency) residual acceleration [5]. Post-flight analysis of the experimental results has demonstrated that the amount of mixing observed between organic liquids can be explained by the additive response of the system to a multicomponent disturbance.

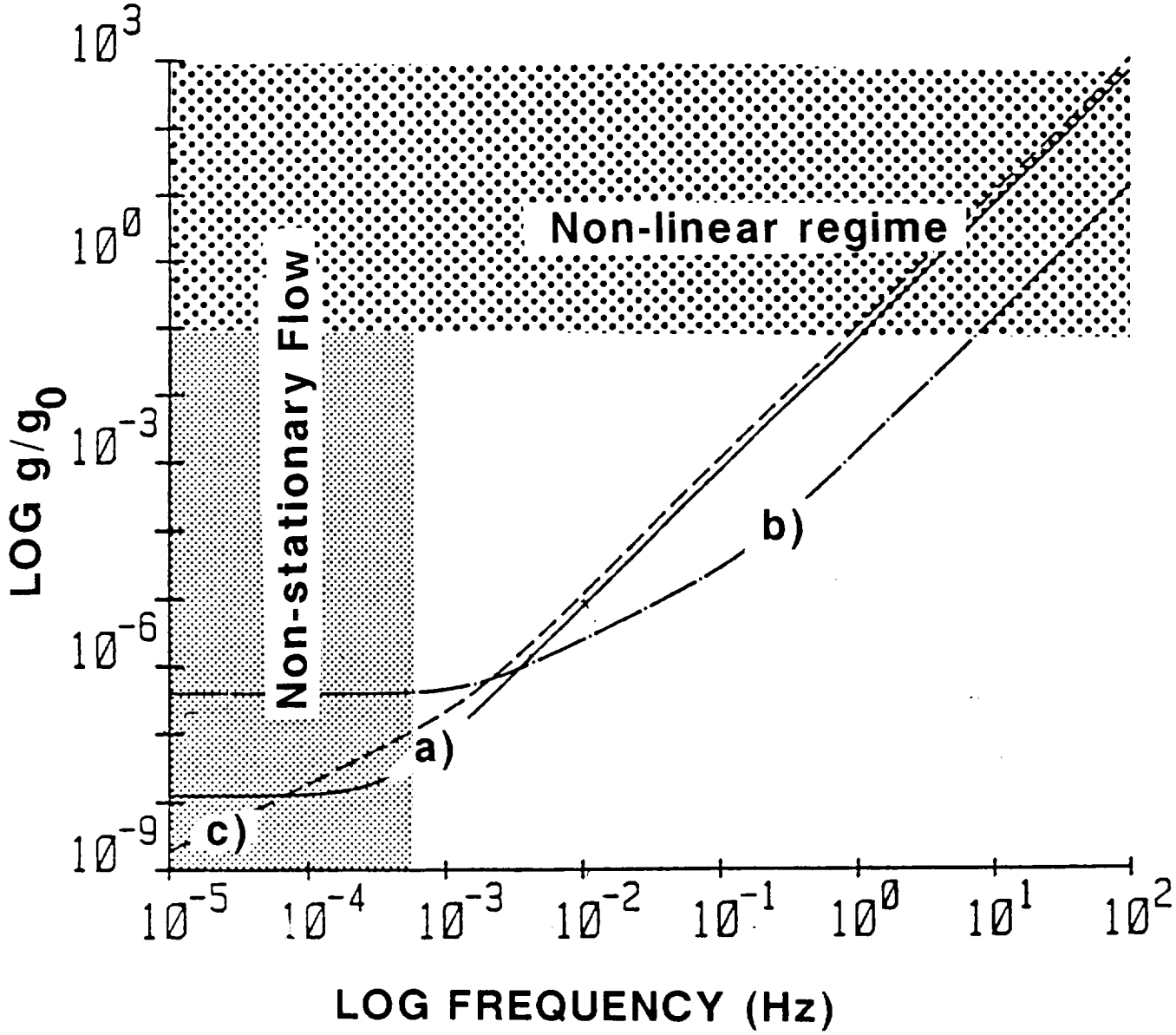

Fig. 1. Tolerable accelerations as a function of frequency for: a) a fluid physics experiment, b) a crystal growth experiment and c) a thermo-diffusion experiment. (After Monti et al. [2].)

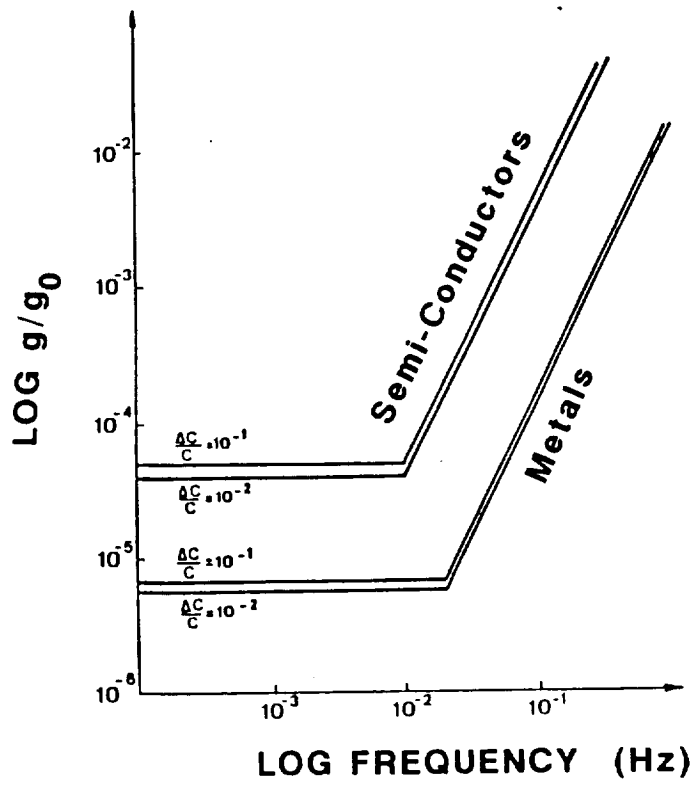

Fig. 2. Tolerable residual accelerations for semiconductor and metal solidification experiments. The sensitivity parameter is longitudinal segregation, $\Delta c/c$. (After Monti et al. [2])

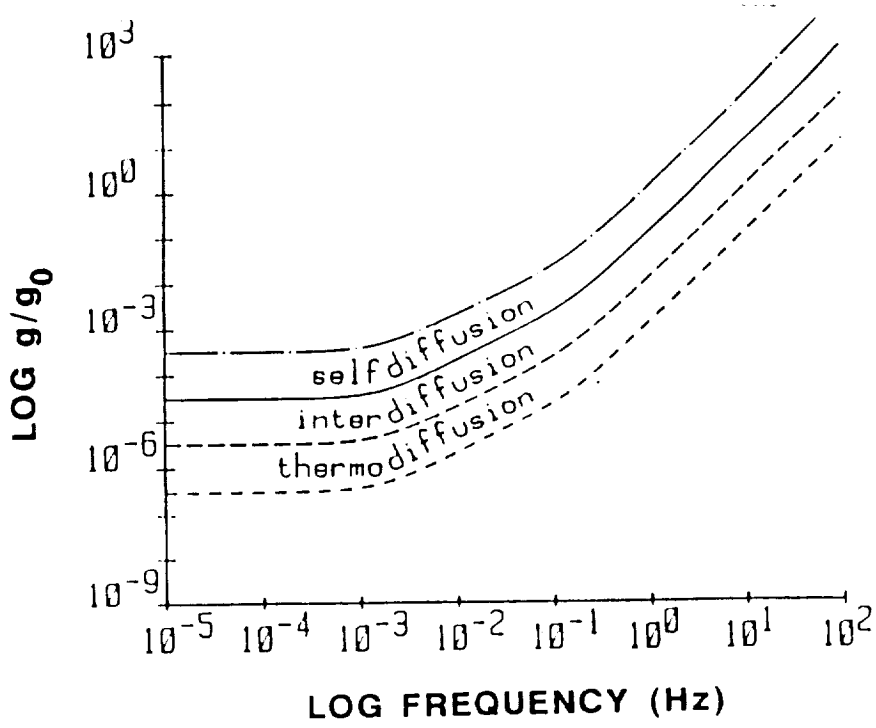

Fig. 3. Tolerable residual accelerations for diffusion experiments. After Monti et al. [2].

Recent work indicates that such an additive effect can also occur during directional solidification [6,7].

In many cases an *a priori* choice of length or time scales may not be obvious. For example, in a study of dopant (solute) uniformity in directionally solidified crystals, the OM estimates of Camel and Favier [9] are in agreement with the direct numerical simulations of Chang and Brown [10] for a Schmidt number (ratio of the melt's kinematic viscosity and dopant diffusivity) of fifty (see Figure 4) but overestimate the amount of radial segregation for a Schmidt number of ten.

2.2 Estimates for thermo-capillary flows

The dimensionless groups associated with mixed thermo-capillary convection and buoyancy-driven convection are [1]:

The dynamic Bond number:	$B = \rho g L^2/\gamma_T$
The Marangoni number:	$Ma = \gamma_T \Delta T L/\mu\kappa$
The Grashof number	$G_r = \Delta T \beta g L^3/\nu^2$
The Prandtl number	$Pr = \nu/\kappa$
The surface Reynolds number	$R_s = MaPr^{-1}$,

where ρ is the mass density, g is the acceleration magnitude; ΔT, and L are, respectively, a characteristic temperature difference and length, β is the coefficient of thermal expansion, ν is the kinematic viscosity, μ is the shear viscosity, γ is the surface tension, γ_T is the derivative of γ with respect to temperature and κ is the thermal diffusivity. The relative importance of gravity and thermo-capillary forces can be estimated as follows [4]:

First, the velocity reference scale is obtained from a consideration of the balance of force tangent to a free surface parallel to the x-axis of a Cartesian coordinate system

$$-\mu\frac{\partial\tilde{u}}{\partial\tilde{x}} = \frac{\partial\tilde{\gamma}}{\partial\tilde{z}} = \left|\gamma_T\right|\frac{\partial\tilde{T}}{\partial\tilde{z}}\,, \tag{2.6}$$

where "~" denotes a dimensional quantity. If the velocity and temperature are scaled by V and ΔT, and $\tilde{x}$ and $\tilde{y}$ are scaled by a characteristic length L, then (2.6) can be recast in the form

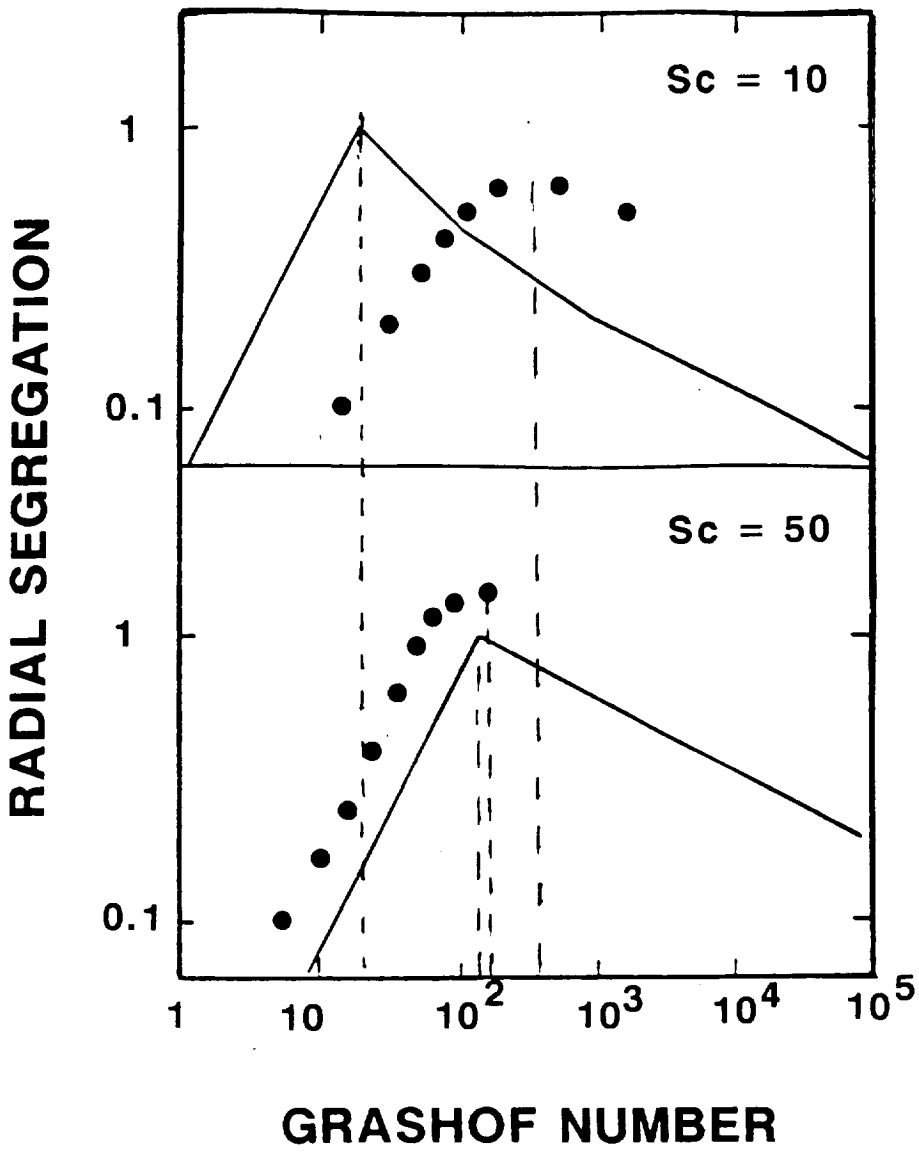

Fig. 4. Comparison of *a priori* estimates (curves) with numerical simulations (dots) [10]. (After Camel and Favier [9].)

$$-\frac{\partial u}{\partial x} = \left(\frac{|\gamma_T|\Delta\tilde{T}}{\tilde{\mu}V^*}\right)\frac{\partial\theta}{\partial z}, \tag{2.7}$$

where u and θ represent the dimensionless velocity and temperature.

For terms on both sides of (2.7) to be of the same order, the magnitude of V^* must be [1,4]

$$V^* = \frac{|\gamma_T|\Delta T}{\mu}. \tag{2.8}$$

The balance of linear momentum and energy in a Boussinesq fluid are given by

$$\frac{\partial\tilde{\mathbf{v}}}{\partial\tilde{t}} + (\mathrm{grad}\tilde{\mathbf{v}})\tilde{\mathbf{v}} = -\frac{1}{\rho}\mathrm{grad}\ \tilde{p} + \nu\Delta\tilde{\mathbf{v}} + \beta_T\tilde{T}\mathbf{g}(\tilde{t}), \tag{2.9}$$

$$\frac{\partial\tilde{T}}{\partial\tilde{t}} + \mathrm{grad}\tilde{T}\cdot\tilde{\mathbf{v}} = \kappa\Delta\tilde{T}. \tag{2.10}$$

For steady flows, Ostrach [1] used (2.8) to scale (2.9). For an aspect ratio of 1 and with $R_s \ll 1$ he obtained:

$$\Delta\mathbf{v} = -\mathrm{grad}\ p + \frac{G_r}{R_s}\mathbf{g}(t), \tag{2.11}$$

where the pressure is scaled with $\mu V^*/L$.

For $R_s \gg 1$ a boundary layer scale, $\delta = L/R_s^{1/2}$, was employed to scale the coordinate perpendicular to the free surface. For this steady boundary layer situation the component of (2.9) perpendicular to the interface has the form

$$u\frac{\partial v}{\partial x} + v\frac{\partial v}{\partial y} = -R^{2/3}\frac{\partial p}{\partial y} + \frac{1}{R_s^{2/3}}\frac{\partial^2 v}{\partial x^2} + \frac{\partial^2 v}{\partial y^2} + \frac{G_r}{R_s}\mathbf{g}(t). \tag{2.12}$$

At small values of R_s the relative contribution of the buoyancy force to convection can be estimated from the ratio G_r/R_s. For large values of R_s, the relative importance of buoyancy is found upon

comparing the buoyancy term with the pressure gradient and is expressed via the ratio $G_r/R_s^{5/3}$. Tables 1 and 2, presented below, give values of these ratios for actual space experiments which will be discussed later in section 2.3.

In order to estimate the effect of time-dependent periodic accelerations on thermo-capillary flows we now extend the approach of Langbein and Tiby (see [2]) beyond a consideration of bouyancy effects alone. The magnitude of the velocity caused by an acceleration occurring with a circular frequency ω is expressed as (see also eq. 2.3)

$$V_g \approx \frac{\beta_T \Delta T g}{(\omega^2 + \frac{\nu^2}{L^4})^{1/2}} \tag{2.14}$$

If thermo-capillary flow is to dominate, the ratio of V_g to V^* must be less than one. For this to occur, the magnitude of the periodic acceleration must satisfy:

$$g < |\gamma_T| \frac{(\omega^2 + \frac{\nu^2}{L^4})^{1/2}}{\mu \beta_T} . \tag{2.15}$$

Eq. (2.15) can be re-interpreted in terms of the ratio of the Grashof number, Gr, and the surface Reynolds number, R_s.

The condition that buoyancy and thermo-capillary forces are of the same magnitude is

$$G_r = R_s(S_t^2 + 1)^{1/2} \tag{2.16}$$

where $S_t = \omega L^2/\nu$ is the Strouhal number. This condition is illustrated graphically in Fig. 5. Three regimes of interest are identified. These regions are defined by the relative values of the Grashof, Strouhal and surface Reynolds numbers. In region I, the Strouhal number S_t is less than one, and the condition that thermo-capillary forces dominate is equivalent to that for a steady flow. In region II, S_t is greater than one. In this region, for a fixed value of R_s, the value of Gr required to give buoyancy forces equal weight to thermo-capillary forces increases with increasing values of the Strouhal number. This essentially reflects the fact that the characteristic time for the fluid response greatly exceeds the period of the disturbance. Thus, thermo-capillary forces dominate

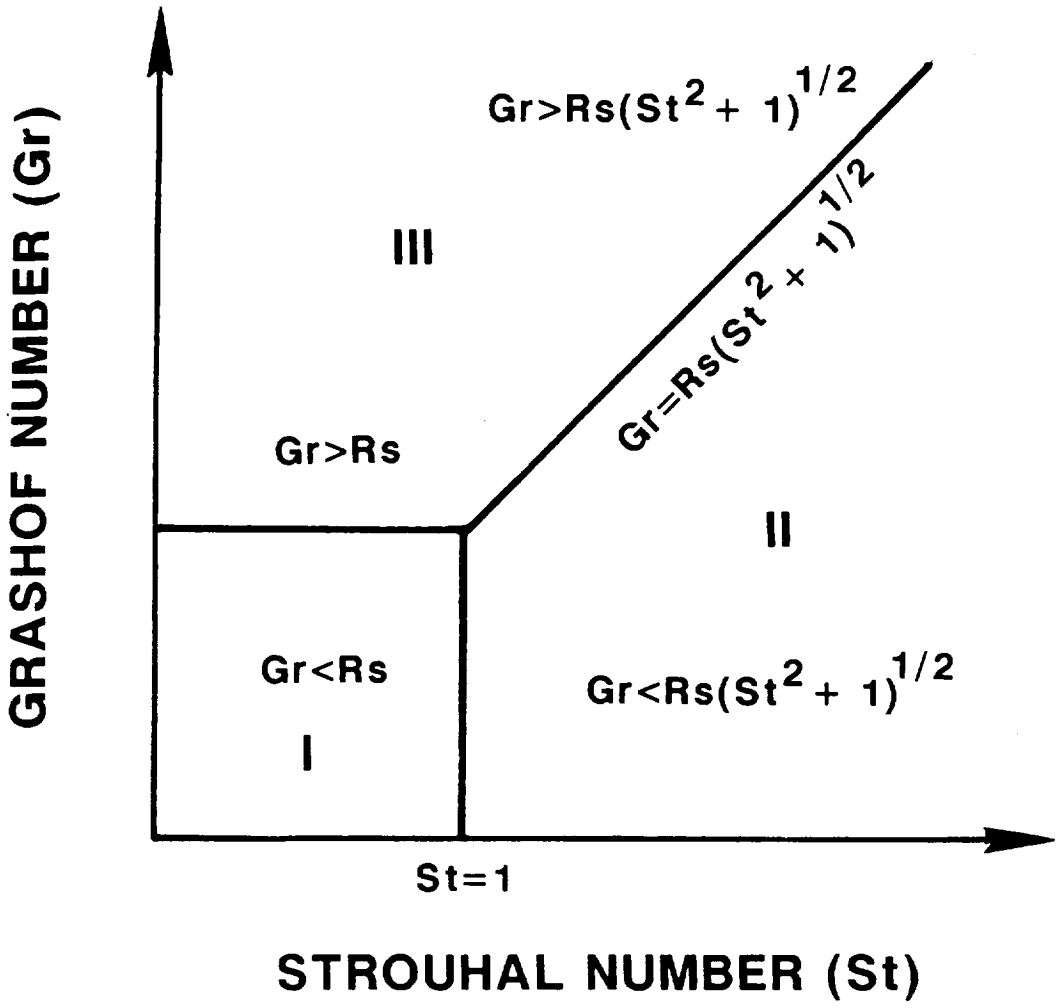

Fig. 5. Generic diagram of flow regimes for mixed thermo-capillary and buoyancy-driven flows. The Strouhal number characterizes the time-dependent effective gravity.

at higher values of Gr than in region I. In region III buoyancy forces predominate over thermo-capillary forces.

Figs. 6 and 7 depict the relationship between the estimated tolerable g-level and the frequency of the acceleration for the physical properties given in Tables 1 and 2 below. The curves have been determined for the following sensitivity criteria; in Fig. 6 the tolerable acceleration levels are such that the buoyancy forces should a) not exceed thermo-capillary forces and b) not exceed 10% of the thermo-capillary forces.

Table 1. Physical Properties

Experiment	1	2	3
Property			
μ [gcms^{-1}]	$4.56(10)^{-2}$	$5.8(10)^{-3}$	$2.82(10)^{-2}$
ν [cm^2 s^{-1}]	$5.01(10)^{-2}$	~$6.0\ (10)^{-3}$ §	$1.48(10)^{-2}$
κ [cm^2 s^{-1}]	$8.7(10)^{-4}$	$1.08(10)^{-3}$	$1.67(10)^{-3}$
γ_T [dyne cm^{-1}K^{-1}]	$6.27(10)^{-2}$ *	$7.7(10)^{-2}$	$-5.7(10)^{-2}$
ΔT [K]	32	7.6 -10	15 - 28
β_T [K^{-1}]	$1.05(10)^{-3}$	10^{-3} #	$-3.8(10)^{-4}$
L [cm]	3.8	1	0.5
Dimensionless Groups			
Gr	$7.2x10^{-5}$ gal - $2.5x10^6$	$2.7(10)^5$ gal	$3(10)^3$~gal - $6(10)^3$ gal
Re_σ	$3.34x10^3$	$2.2(10)^4$	$1\text{-}2(10)^4$
Gr/Re_σ	~$2x10^2$ gal	12 gal	~1.5- 6 gal
$Gr/(Re_\sigma)^{5/3}$	~ 1 gal	$1.6(10)^{-2}$ gal	$1\text{-}3(10)^{-2}$ gal
Pr	57-70#	~6	8.9

1 -Napolitano et al. [12], 2- Chun [15], 3- Schwabe and Scharmann [13]

§Obtained using a density estimated from values given in the CRC Handbook of Chemistry and Physics, 64th edition.

*The value has been inferred from maximum velocity data given in [12] and as such cannot be considered precise.

Estimated.

In Fig. 7 the buoyancy forces should not exceed a) 10% and b) 1% of the thermo-capillary forces. These figures represent estimates based

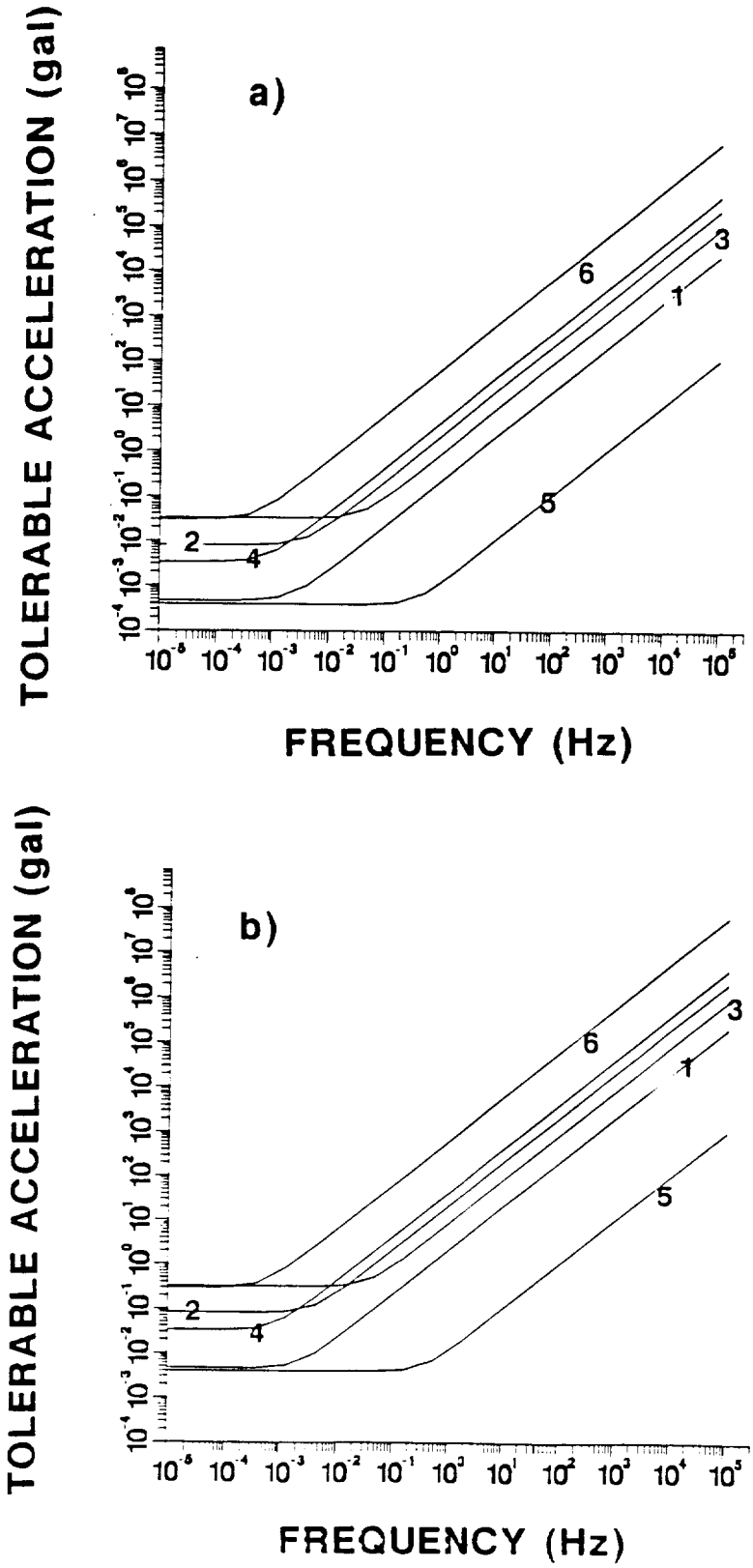

Fig. 6. Sensitivity of experiments listed in tables 1 and 2
a) buoyancy and thermo-capillary forces equal magnitude
b) buoyancy forces 10% of thermo-capillary forces (calculations based on penetrative flow scales).

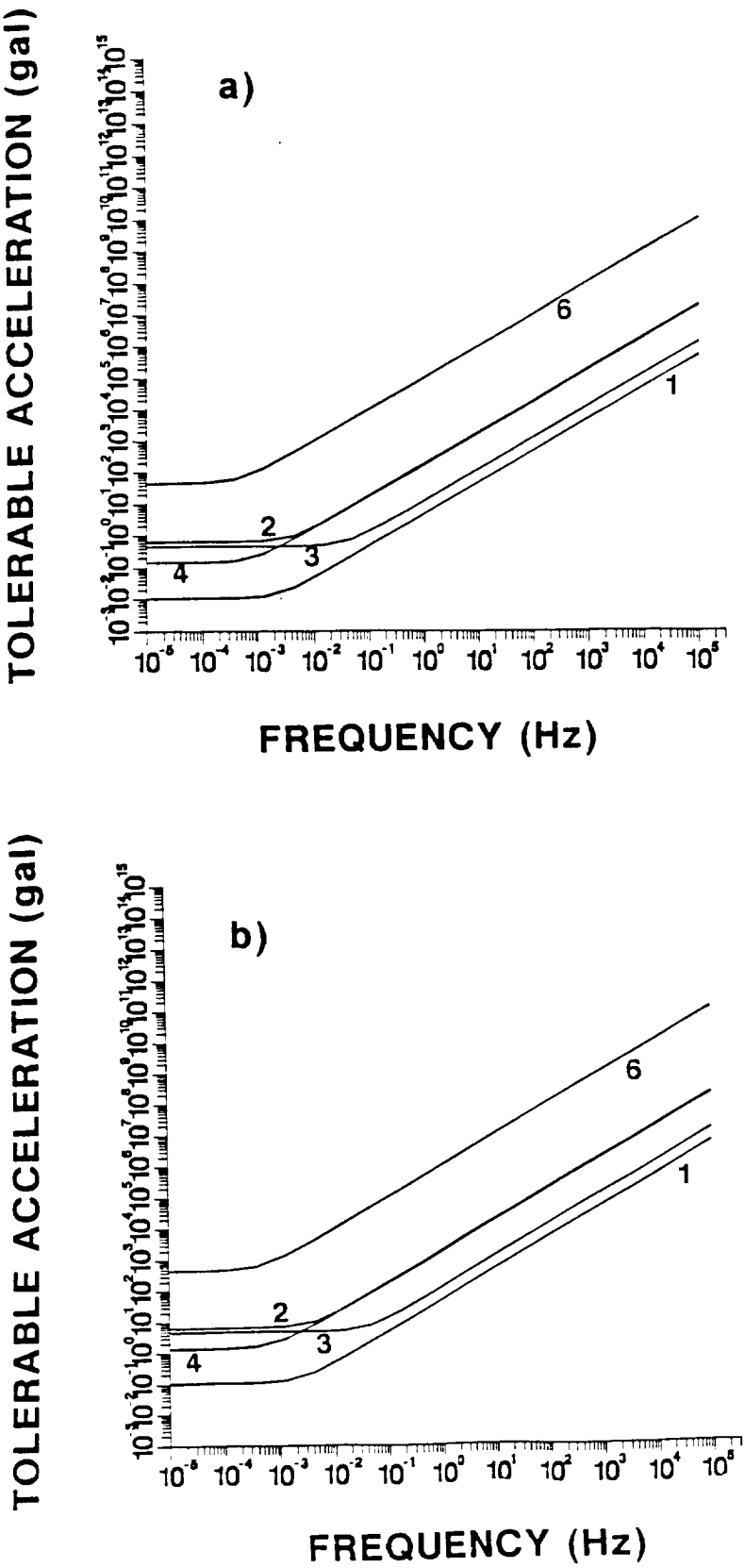

Fig. 7. Sensitivity of experiments listed in tables 1 and 2
a) buoyancy forces 10% of thermo-capillary forces,
b) buoyancy forces 1% of thermo-capillary forces
(calculations based on boundary layer flow scales).

on two extremes of flow regime, penetrative or "viscous" flow (Fig. 6) and boundary layer flow (Fig. 7). They may be respectively considered as "worst" and "best" case estimates for the given sensitivity parameters. The results for the penetrative regime are independent of the temperature difference ΔT, while for the boundary layer scaling the tolerable acceleration depends on $(\Delta T)^{-2/3}$. The low frequency (< 10^{-2} Hz) acceleration environment predicted for the space station should not exceed levels of 10^{-5} gal [53]. Higher frequencies can be associated with acceleration magnitudes of up to 10^{-2} gal. In terms of these predicted levels or those measured on past missions [54], the practical sensitivity range is restricted to disturbances with frequencies in the range 10^{-1} - 10 Hz. The majority of the estimates suggest that periodic vibrations will generally not lead to significant buoyancy effects in thermo-capillary experiments such as those considered here. This may not be the case for isolated impulse disturbances.

Table 2. Physical properties for materials science related thermo-capillary flow experiments.

Experiment	4	5	6
Property			
μ [gcms^{-1}]	$1.94(10)^{-2}$	5.3	$7.5(10)^{-3}$
ν [cm^2 s^{-1}]	$2.76(10)^{-3}$	1.33	$3.0(10)^{-3}$
κ [cm^2 s^{-1}]	$2.17(10)^{-3}$	$4.0(10)^{-4}$	$1.3(10)^{-1}$
γ_T [dyne cm^{-1}K^{-1}]	$-6.2(10)^{-2}$	$-7.7(10)^{-2}$	$-4.3(10)^{-1}$
ΔT[K]	5	5	50
β_T [K^{-1}]	$1.21(10)^{-4}$	$2.23(10)^{-3}$	$1.43(10)^{-4}$
L [cm]	1.5	1.5	2.0
Dimensionless Groups			
Gr	$2.6\text{x}10^5$ g/g$_o$	22 g/g$_o$	$6.5(10)^6$ g/g$_o$
Re$_\sigma$	$8.684\text{x}10^3$	$8.2(10)^{-2}$	$2(10)^6$
Gr/Re$_\sigma$	30g/g$_o$	254 g/g$_o$	3.25 g/g$_o$
Gr/(Re$_\sigma$)$^{5/3}$	$7(10)^{-2}$ g/g$_o$	-	$2(10)^{-4}$ g/g$_o$
Pr	$1.27(10)^{-2}$	595	2

4- Lind [24] (indium), 5- Lind [24] (selenium), 6- Cröll et al. [22]

It is clear that in a low gravity environment the magnitude of the Grashof number will be reduced in comparison to terrestrial conditions. Whenever G_r/R_s or $G_r/R_s^{5/3}$ are less than unity, thermo-capillary flow should be expected to dominate. Then the estimates discussed here provide some insight as to the extent to which small but finite accelerations might affect surface-driven flows. However, even under these conditions, the extent to which buoyancy-driven convection affects the symmetry and time-dependence of thermo-capillary flows is unclear and is best examined via numerical modelling.

2.3 Observed response of thermo-capillary experiments

A free-fall experiment in a drop tower [11] first confirmed the existence of capillary flows in low gravity. Several space flight experiments have since been concerned with thermo-capillary driven convection [1,3,4,12-15]. The transition from laminar to oscillatory convection has been studied by Schwabe and Scharmann [13], and Chun [15] has examined the nature of oscillatory thermo-capillary flow in cylindrical liquid bridges with different aspect ratio. These authors have reported that the transition from steady to oscillatory flow occurs at Marangoni numbers of 10^4 . On the D-1 mission (1985), Napolitano et al. [12] studied thermo-capillary flow in cylindrical liquid bridges but did not observe oscillatory flow despite the fact that the Marangoni number was of the order 10^4. The origins of the oscillations are not well understood. It has been proposed that oscillations are either related to interaction between convective heat transfer in the bulk fluid and the surface temperature gradient [15] or are controlled by the surface flexibility [17]. A measure of this flexibility is given by $S = Pr^{-1}(\gamma_T \Delta T/\sigma)$ and it is suggested [17] that the absence of oscillations in Napolitano's D1 experiments is because S is too small. Unfortunately, the value of σ in the experiment is not given. However, if S being small is the sole reason for oscillations then its value must be less than 1.5×10^{-3}, which is the value for the experiment of Schwabe and Scharmann [13]. At present, the origin of the differences in the experimental results cannot be explained well (from a rigorous theoretical viewpoint). It should be emphasized, though, that the contention that S controls the oscillations is based both on experimental observations [18] and on scaling arguments which suggest that the oscillation originates in corner regions. If the free

surface shape plays a dominant role, the influence of residual accelerations on the surface shape needs to be considered. This is dealt with in the next section.

Napolitano et al. [12] report a lack of correlation between experiment and their theoretical calculations, that is not well understood. The authors point out that this could be due to residual gravity levels. In fact, closer examination of their observed streamline patterns indicates that the flows were not axisymmetric (a basic assumption for their model calculations). Figures 6 and 7, and Table 1 give estimates of the relevant dimensionless groups and g-tolerance curves for the three thermo-capillary flow experiments mentioned above. If the boundary layer scales are correct, the buoyancy forces would only be one percent of the capillary forces for a residual acceleration of 10^{-2} gal[1]. If, in fact, the ratio Gr/Re_σ is the correct group, a residual acceleration of 10^{-2} gal could affect the experiment to a considerable extent for disturbances with frequencies of up to 2 Hz. Very low frequency residual accelerations (< 10^{-2} Hz) generally have amplitudes smaller than 10^{-3} gal. Thus, it is unlikely that residual accelerations in this frequency range would exert a significant influence on the flow as far as these three experiments are concerned. The most sensitive frequencies sensitivity lie in the range of 10^{-1} Hz to 10 Hz.

For experiments designed to examine the conditions under which thermo-capillary flow transitions can occur, the effects of residual gravity could also be important. For example, the interplay between gravity and the dependence of surface tension on temperature is well understood for the onset of mixed buoyancy- and thermo-capillary-driven convection [19-21]. This interaction is expressed through the Rayleigh and Marangoni numbers at the onset of instability:

$$Ra^*Ma_c + Ma^*Ma_c = Ra_cMa_c \qquad (2.17)$$

where the subscript 'c' denotes the critical values of the Rayleigh and Marangoni numbers for the onset of pure buoyancy-driven flow or pure thermo-capillary flow. For a transition to oscillatory flow it should be considered that even if the contribution to the fluid velocity due to residual gravity is small, non-linear interaction between the thermo-

[1] 1gal = 9.8 m s^{-2}

capillary driven motion and the buoyancy-driven flow could affect the nature of the critical conditions at which the transition occurs. Furthermore, and perhaps more importantly, the early stages of an experiment[1] may be strongly influenced by the residual gravity and thereby affect the outcome of the experiment. For example, the desired transition point from which the steady conditions bifurcate may not be obtained.

In addition to the fluid physics community, crystal growers are also interested in thermo-capillary flows since they are inherent in the floating zone and open-boat methods of crystal growth [22-25]. As a consequence, even at zero-g, for multi-component or doped melts these techniques will always lead to convective effects on (component) or dopant redistribution. In terms of the properties of the solidified material microgravity float zone processes are attractive mainly for the purification or zone refining of single component materials. In particular, the low-gravity environment allows for longer stable zones that cannot be produced on earth.

The spacecraft environment will not lead to the elimination of convective effects since only buoyancy will be reduced or practically eliminated. However, Cröll et al. [22] have demonstrated the use of the microgravity environment to conduct floating zone crystal growth experiments with coated and uncoated zones. The coated zones led to the elimination of thermo-capillary flow, while essentially retaining a deformable surface. This allowed a comparison between ground-based experiments dominated by mixed thermo-capillary/buoyancy-driven flow (uncoated), buoyancy-driven flow (coated) and space experiments dominated by thermo-capillary flow (uncoated) and diffusion (coated). This type of comparative experiment allows for greater understanding of the float zone crystal growth process from a ground-based standpoint.

The sensitivity of such experiments to the residual acceleration environment has yet to be assessed. Table 2 gives estimates of the dimensionless groups associated with the float zone solidification experiments described in references [22-25]. Figs. 6 and 7 depict the corresponding tolerable acceleration curves according to eq. (2.15). Based on these estimates it is unlikely that the experiment of Cröll et al. would have been affected by buoyancy-driven flow. Lind's experiment involving selenium melts appears to be the most sensitive

[1]For example, the initial transient stages of an experiment where the rigid wall temperatures are adjusted to their desired values.

to residual accelerations. As with the experiments described earlier, the estimates suggest that disturbances in the 10^{-2} - 10 Hz frequency range are likely candidates to cause significant response. It should be borne in mind, however, that these estimates do not account for the rate of zone translation which will also have an influence on the nature of any fluid motion in the melt.

2.4 Estimates of liquid zone sensitivity

Experiments involving free surfaces of liquids have a high probability of responding to residual accelerations. Indeed, unexpected results have been attributed to residual accelerations in several cases [26-29]. Particular examples of such experiments involve liquid (float) zones. Following Sekerka and Coriell, [30] we examine three types of liquid zone:

(i) isothermal zones suspended between inert solids
(ii) non-isothermal zones suspended between inert solids
(iii) (crystal growth) non-isothermal zones suspended between a feed rod and a growing crystal.

Each of these types of experiment has been, and will continue to be, undertaken in space laboratories.

(i) Isothermal zones suspended between inert solids

The dimensionless group associated with the shape of static liquid zones is the Static Bond number, $B_o = \rho g_o L^2 / \gamma$, where γ is the surface tension, L is the zone length, ρ is the liquid density and g_o is the (steady) acceleration. It expresses the relative importance of gravitational and surface forces. A dynamic Bond number $B_n = \rho g_n L^2/\gamma$, where g_n is the amplitude of the n^{th} component of the residual acceleration, can also be defined. A comprehensive description of stable zone shapes in zero gravity and as a function of B_o has been given by Martinez et al. [31]. Fig. 8 displays their results for the stability of static zones with a steady acceleration parallel to the zone axis. For B_o= 0, the zone volume $V=V^*= \pi R^2 L$ and contact angle $\alpha = 90^o$ the maximum stable length is $2\pi R$ (the "Rayleigh limit"). Coriell et al. [32] investigated the effect of B_o on the maximum length of such zones and compared theoretical predictions with experimental results (see Fig. 9). The actual length of the equilibrium zone is determined by the volume, the contact angle α and the static Bond number.

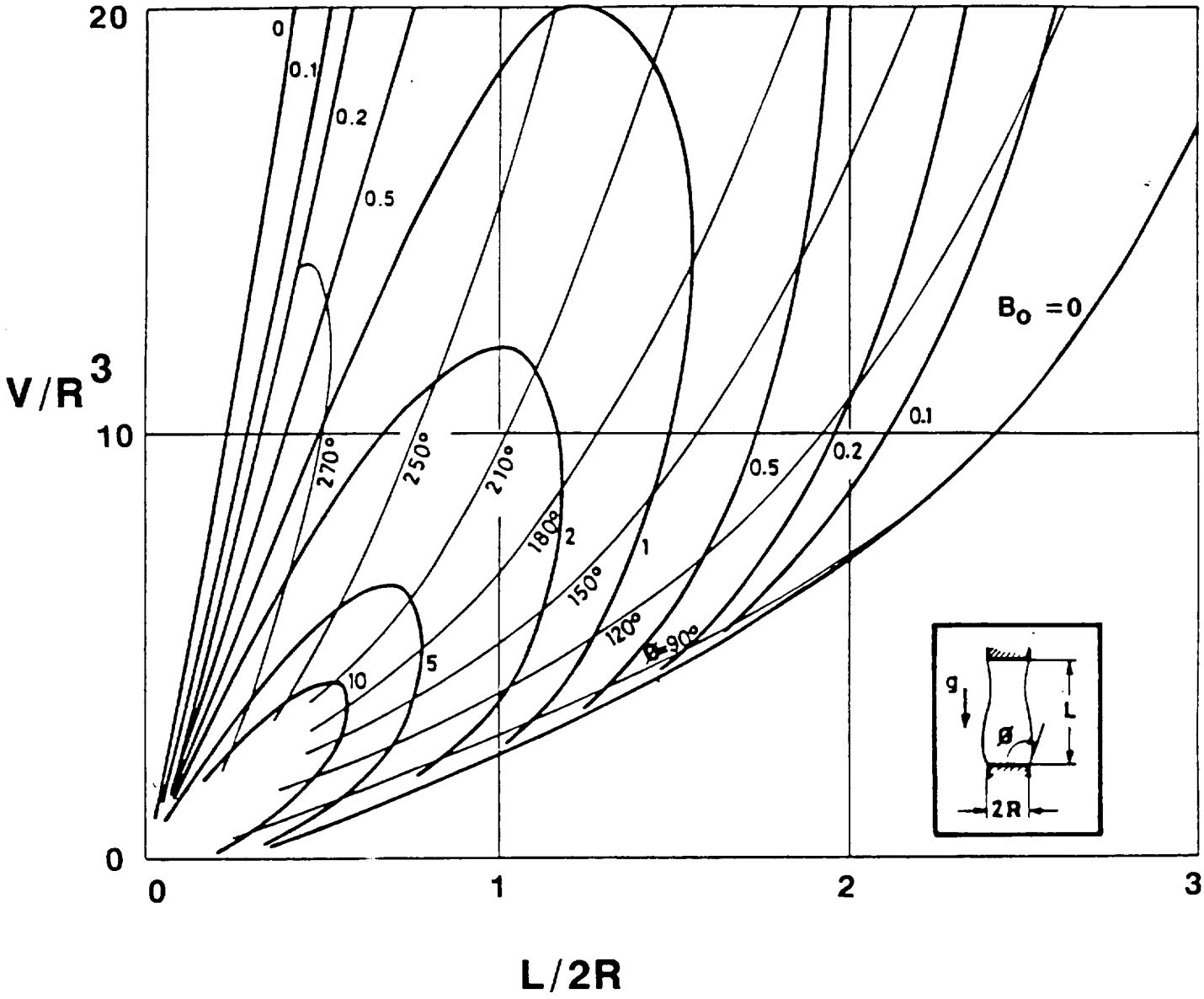

Fig. 8. Stability limits for a liquid zone of volume V, length L and radius R undergoing a constant axial acceleration characterized by given values of the Bond number B_o. The angle φ is defined in the inset. (After Martinez et al. [31].)

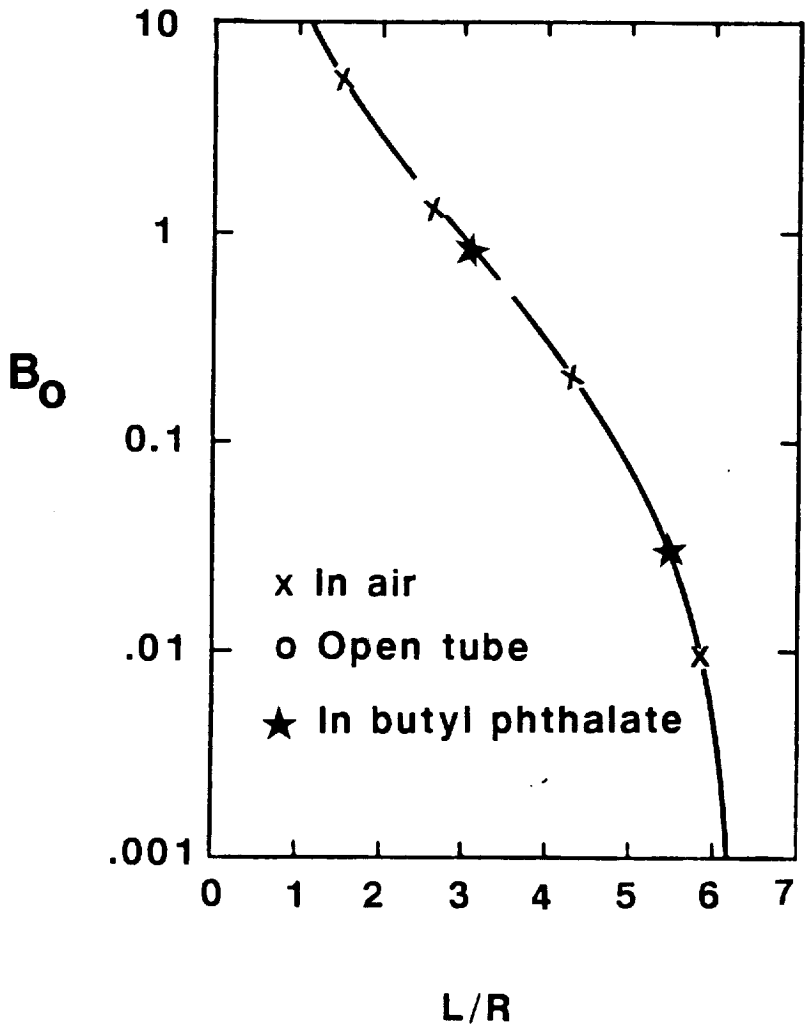

Fig. 9. Comparison of theory and experiment for the maximum stable zone length, L, as a function of the Bond number B_o, for an isothermal liquid zone (with a constrained volume equal to $\pi R^2 L$) suspended between inert solids of radius R undergoing a constant axial acceleration. (From Sekerka and Coriell [30].)

Estimates of the effect on the free surface shape of oscillatory residual acceleration parallel to the axis of a liquid bridge have been made by Langbein [33]. His calculations suggest that the sensitivity of the surface to residual accelerations is highest for disturbances with frequencies close to the natural frequency of the bridge. The zone shapes appear to be most sensitive to frequencies in the 0.001-10 Hz range. For the example given in [33], the maximum (oscillatory) acceleration magnitudes that can be tolerated by a bridge less than 90% of the maximum stable bridge length (given by the Rayleigh limit) range from 5×10^{-8} to 5×10^{-3} gal. Recent calculations [34] suggest that non-linear interactions cannot be ignored and that for excitation (i.e. acceleration) frequencies corresponding to eigenfrequencies of the zone non-linear effects can be significant. The sensitivity of bridges to time-dependent accelerations perpendicular to the free surface has yet to be examined.

(ii) Non-isothermal zones suspended between inert solids

If the zone is not isothermal, the equilibrium conditions referred to above no longer hold. In this case, the five dimensionless groups introduced earlier in section 2.2 govern the problem. For molten silicon, Sekerka and Coriell have calculated the values of these groups. They are presented in Table 3.

Table 3. Values of dimensionless groups for silicon calculated from the data of Chang and Wilcox [35]. The length scale is taken to be the zone radius R; β is estimated at 1.6×10^{-4} K^{-1}. For earth, g_E is taken as 9.8 m/sec^2 and for space, g_S is taken as $10^{-4}g_E$. ΔT is assumed to be 10 C°. (After Sekerka and Coriell [30].)

	B_o	Gr	$N_3 = \frac{\rho v^2}{R\sigma}$	$R_s N_3$	Pr	R_s
EARTH						
R = 1 cm	3.4	1.3×10^{5}	4.3×10^{-8}	6×10^{-3}	2.3×10^{-2}	1.4×10^{5}
R = 10^{-2} cm	3.4×10^{-4}	1.3×10^{-1}	4.3×10^{-10}	6×10^{-3}	2.3×10^{-2}	1.4×10^{3}
SPACE						
R = 1 cm	3.4×10^{-4}	1.3×10	4.3×10^{-8}	6×10^{-3}	2.3×10^{-2}	1.4×10^{5}

The relative magnitudes of the terms suggest that on earth the zone shape will be dominated by the capillary effect (large B_o) for typical zone sizes, while under low gravity conditions the zone shape will be influenced mainly by the temperature gradient along the interface. In addition, consideration of the dynamic Bond number B_n and the surface Reynolds number suggests that dynamic distortions may also be important.

(iii) Crystal growth: non-isothermal zones suspended between a feed rod and a growing crystal.

Consideration of the float zone (FZ) crystal growth process introduces further complications which ultimately require independent analyses. In the previous cases, the inert solids between which the zone is suspended usually have a planar contact surface with the melt. This is generally not the case for the crystal growth process. The actual shape depends primarily on the thermal conditions. The influence of the meniscus angle at either of the crystal-melt-vapor tri-junctions can also be significant and has been analyzed by Heywang [36] and Coriell et al. [37]. In addition to zone failure due to the classical capillary instability, a "dewetting" instability is also found to be important. The instability arises when the angle between the meniscus and the melt-crystal interface is less than the wetting angle for the liquid melt on the solid crystal. For Si zones of greater than 1 cm radius zone failure on earth occurs due to the Heywang instability [37,38]. Zone failure by this mechanism is unlikely under low gravity conditions.

2.5 Observed response of liquid zone experiments

Martinez [26] and Haynes [27] comment on the effects of an attitude change during experiments on Spacelab 1. The experiments involved the study of liquid column stability and liquid spreading kinetics. The residual acceleration environment had a noticeable effect on stationary fluid masses. Roll rates of 0.13° per second were apparently "... sufficient to interfere strongly with some of the fluid configurations studied in the FPM..." [29]. Later experiments on D-1 which involved static and rotating liquid columns also experienced some interference that has been attributed to the residual acceleration environment. Martinez [28] recorded the following interference apparently caused by the residual acceleration environment:

Run 1: During the initial stages of the first run (designed to establish a long cylindrical column by liquid injection) a wide deformation of the bridge was observed in response to shuttle maneuvers. The P.I. reports that the zone would certainly have broken had it been more slender.

Run 5: prior to rotation of the supporting discs a 10cm column exhibited a pronounced random oscillation.

Run 6: the goal of the experiment was to excite a c-mode deformation [28] of the bridge. An amphora mode [28] resulted. The explanation proposed by the P.I. was that the residual acceleration environment caused a shift in the stability limits. The maximum residual acceleration recorded during these experiments was 10^{-4} gal.

We have expressed Bond numbers in terms of g/g_0 for the physical properties of liquid columns used in two past space experiments in Table 4. The estimates indicate that the experiment involving the long liquid bridges should be more sensitive. In contrast to Martinez, none of Padday's experiments were reported to have been affected by the residual accelerations.

Table 4. Dynamic Bond numbers estimated for two D-1 liquid zone experiments in which 5 cs silicone oil was used.

	Martinez [28]	Padday [29]
ρ [g cm^{-3}]	0.92	0.92
L [cm]	10	1.5
σ [dyne cm^{-1}]	0.2	0.19
B_n	$4.5(10)^{-4}$ g_n/g_0	$7.1(10)^{-3}$ g_n/g_0

3. Liquid zone/float zone shape sensitivity: numerical analysis

3.1 Introduction

Both the fluid physics and the crystal growth community have an interest in the sensitivity of liquid zones to residual accelerations. Whether the particular space flight experiment involves the study of isothermal zone shapes, or attempts to utilize the low gravity environment to maximize the length of the liquid zone in a float-zone crystal growth experiment, the effects of residual acceleration must be considered [31].

We have formulated a simple non-linear 1-D model of an isothermal liquid zone has been formulated and used to examine the effect of g-jitter oriented parallel to the zone axis. This allows an examination of interaction between various components of a typically complex residual acceleration without the restriction that the response necessarily be linear. The model is based on a formulation developed by Lee [39] which has been successfully applied to several types of liquid bridge problems [40-46].

We have examined the effects of single frequency g-jitter disturbances. The sensitivity is expressed in two ways: firstly *zone breakage*, defined in terms of the conditions under the radius goes to zero, and secondly in terms of a *shape change criterion* which indicates when the zone deviates more than 10% from its original shape. An optimal searching scheme is used to find the boundary between the regions in parameter space for which the sensitivitiy criterion is or is not satisfied. It is emphasized that the analyses include a steady background acceleration. This background acceleration produces a particular equilibrium zone shape which is characterized by a static Bond number $Bo = \rho g_o L^2 / \gamma$, where γ is the surface tension, L is the zone length, ρ is the liquid density and g_o is the (steady) acceleration.

3.2 Formulation of the model equations

Consider a slender liquid bridge (see Fig. 10) held between two equidimensional rigid circular disks (radius R_0^*) separated by a distance L. The disks are aligned coaxially. The liquid is an isothermal incompressible Newtonian fluid with constant physical properties. It is held in place by capillary forces. Consistent with our aim to isolate the mechanical response of the surface to g(t) acting along the cylinder axis we make the following additional assumptions:

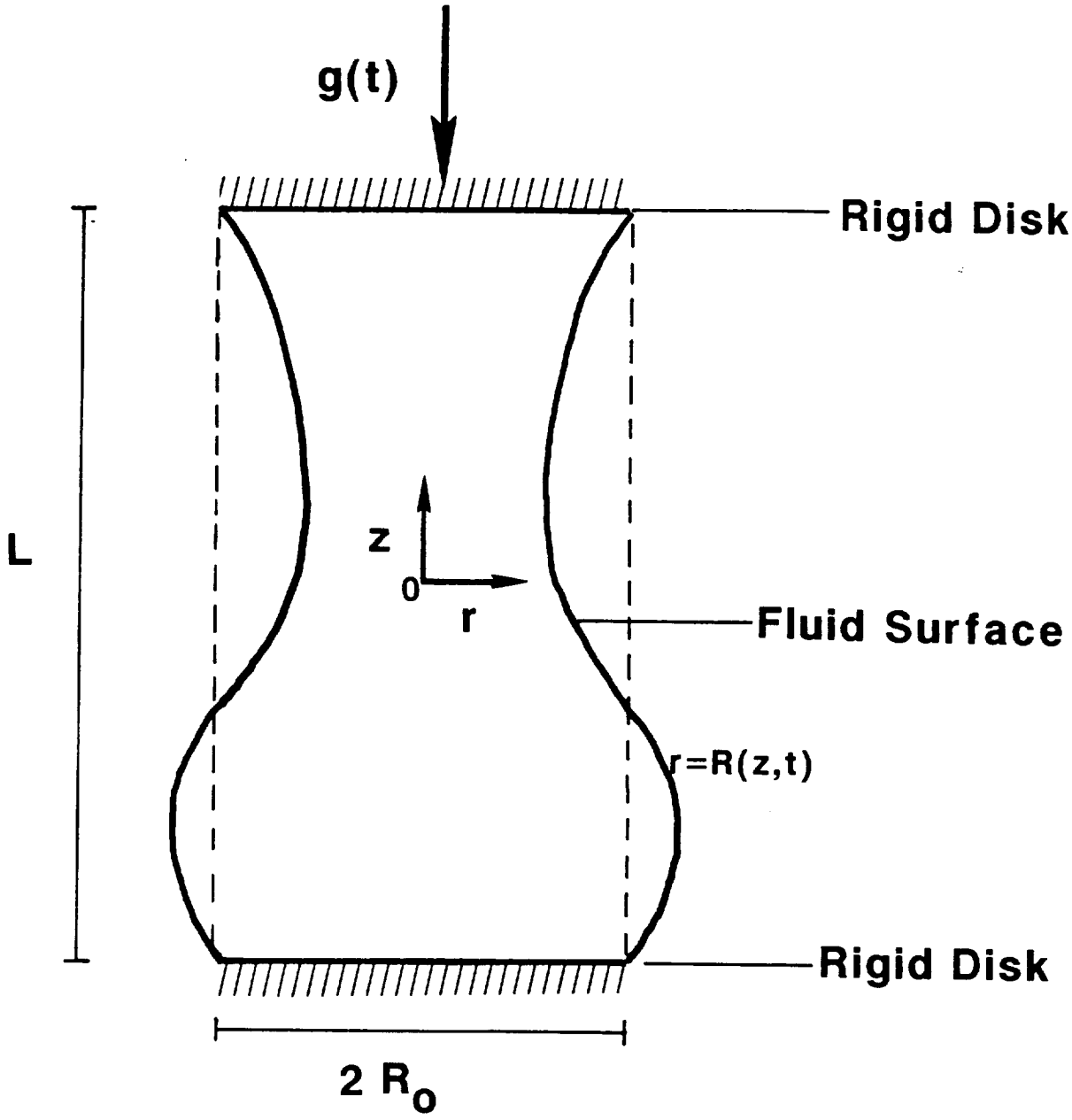

Fig. 10. Idealized liquid zone configuration.

(i) Internal motion of the liquid bridge is caused only by capillary pressure gradients caused by deformation of the interface.

(ii) The effect of the atmosphere around the bridge is negligible.

The governing equations are rendered non-dimensional using R_o, $(\rho R_o^3/\sigma)^{1/2}$, and $R_o(\rho R_o^3/\sigma)^{-1/2}$ to respectively scale distance, time and velocity. Here ρ is the mass density, σ is the surface tension. The dimensionless equations for mass and momentum transfer then take the following form:

In the liquid $(0 < r < R(z,t),\ -\Lambda < z < \Lambda)$,

$$\frac{1}{r}\frac{\partial(ru)}{\partial r} + \frac{\partial w}{\partial z} = 0\ , \tag{3.1}$$

$$\frac{\partial u}{\partial t} + u\frac{\partial u}{\partial r} + w\frac{\partial u}{\partial z} = -\frac{\partial p^*}{\partial r} + C\left(\frac{\partial^2 u}{\partial r^2} + \frac{1}{r}\frac{\partial u}{\partial r} + \frac{\partial^2 u}{\partial z^2} - \frac{u}{r^2}\right), \tag{3.2}$$

$$\frac{\partial w}{\partial t} + u\frac{\partial w}{\partial r} + w\frac{\partial w}{\partial z} = -\frac{\partial p^*}{\partial z} + C\left(\frac{\partial^2 w}{\partial r^2} + \frac{1}{r}\frac{\partial w}{\partial r} + \frac{\partial^2 w}{\partial z^2}\right), \tag{3.3}$$

where p^* is a reduced pressure given by $p^* = p + B_o g(t) z$, and $C = \nu(\rho/\gamma R)^{1/2}$ (with ν the kinematic viscosity) is a measure of the relative strength of viscous and capillary forces. The function g(t) is given by $g(t) = 1 + (B_1/B_o)\cos\omega t$, where ω is the dimensionless frequency, $B_o = g_o\rho R_o^2/\gamma$ is the usual static Bond number, $B_1 = g_1\rho R_o^2/\gamma$ is a dynamic Bond number and $\Lambda = L/2R_o$. The magnitudes of the steady and time-dependent acceleration components are given by g_o and g_1 respectively. The linear frequency of the disturbance is given by $f = \omega(2\pi\rho R_o^3/\gamma)^{1/2}$.

The boundary conditions at the surface r=R(z,t) are

$$p^* - \frac{2C}{(1+R_z^2)}\left[\frac{\partial u}{\partial r} + R_z^2\frac{\partial w}{\partial z} - R_z\left(\frac{\partial w}{\partial r} + \frac{\partial u}{\partial z}\right)\right]$$
$$= \frac{1}{(1+R_z^2)^{3/2}}\left[\frac{1+R_z^2}{R} - R_{zz}\right] + B_o\, g(t) z, \tag{3.4}$$

$$C\left[2R_z\left(\frac{\partial u}{\partial r} - \frac{\partial w}{\partial z}\right)\right] + \left(1-R_z^2\right)\left(\frac{\partial w}{\partial r} + \frac{\partial u}{\partial z}\right)] \;=\; 0, \tag{3.5}$$

which respectively represent the balance of normal and tangential force components at the surface. In addition, there is the kinematic condition.

$$\frac{\partial R}{\partial t} - u + w\,\frac{\partial R}{\partial Z} \;=\; 0. \tag{3.6}$$

The conditions at $z= \pm \Lambda$ are

$$R(z,t) = 1\ , \qquad w(r,z,t) = u(r,z,t) = 0, \tag{3.7}$$

which fixes the contact line between the disk and the liquid and ensures no slip of the fluid in contact with the disk. At r=0 the conditions

$$u(0,z,t) = 0\ ,\ \frac{\partial w}{\partial r}(0,z,t) = 0, \tag{3.8}$$

ensure axisymmetry. The formulation is complete upon specifying suitable initial conditions which we take in the form

$$R(z,0)) \;= R_0(z),\ \ w(r,z,0)=u(r,z,0)=0, \tag{3.9}$$

along with the constraint that the volume remain constant; i.e.

$$\int_{-\Lambda}^{+\Lambda} R_0^2\ (z)\ dz \;=\; \int_{-\Lambda}^{+\Lambda} R^2\ (z,t)\ dz \;=\; 2\,\Lambda. \tag{3.10}$$

The above system of equations defines an unsteady free boundary problem since the location (and hence the shape) of the oscillating interface is *a priori* unknown and must be determined as part of the solution.

3.3 One-dimensional model

In order to calculate the response of the shape of the liquid zone to time-dependent axial accelerations, we approximate the system of equations presented in the last section and formulate a one-dimensional model. This considerably reduces the complexity of the

problem and allows an examination of a relatively wide range of parameters without excessive computation times. Meseguer [40] used a one-dimensional model that holds provided the slenderness Λ is large. (Recall that the slenderness is bounded from above by the Rayleigh limit i.e. $\Lambda_{max} = \pi$.) The axial velocity component w is assumed to depend only on the z coordinate and time. In this case eqs. (3.2) and (3.3) become decoupled and the following system of equations results:

$$\frac{1}{r}\frac{\partial(ru)}{\partial r} + \frac{\partial w}{\partial z} = 0, \tag{3.11}$$

$$\frac{\partial w}{\partial t} + w\frac{\partial w}{\partial z} = \frac{\partial p^*}{\partial z} + C\frac{\partial^2 w}{\partial z^2}, \tag{3.12}$$

Since w is assumed to depend only on z, eq. (3.11) is easily integrated and yields

$$u(r,z,t) = -\frac{r}{2}\frac{\partial w}{\partial z}. \tag{3.13}$$

Following Lee [39] and Meseguer [46] we take $S=R^2(z,t)$ and $Q = S(z,t)w(z,t)$ and substitute (3.13) into the kinematic boundary condition (3.6). This yields

$$\frac{\partial S}{\partial t} + \frac{\partial Q}{\partial z} = 0, \tag{3.14}$$

which expresses conservation of mass at the interface. Similarly, eq. (3.12) can be recast in the form

$$\frac{\partial Q}{\partial t} + \frac{\partial}{\partial z}\left(\frac{Q^2}{S}\right) = -S\frac{\partial p^*}{\partial z} + SC\frac{\partial^2}{\partial z^2}\left(\frac{Q}{S}\right), \tag{3.15}$$

which expresses the conservation of momentum in the axial direction for each cross section of the zone. At the interface, the component of force balance normal to the interface reduces to

$$p^* = \frac{C}{4S + \left(\frac{\partial S}{\partial z}\right)^2}\left[\left(2\left(\frac{\partial S}{\partial z}\right)^2 - 4S\right)\frac{\partial}{\partial z}\left(\frac{Q}{S}\right) + 2S\frac{\partial S}{\partial z}\frac{\partial^2}{\partial z^2}\left(\frac{Q}{S}\right)\right] +$$

$$4\left(4S + \left(\frac{\partial S}{\partial z}\right)^2\right)^{-\frac{3}{2}}\left(2S + \left(\frac{\partial S}{\partial z}\right)^2 - S\frac{\partial^2 S}{\partial z^2}\right) + Bz, \qquad (3.16)$$

where eq. (3.14) and the expressions for S and Q have been used to replace u and w. Together with the following boundary and initial conditions eqs. (3.15) and (3.16) complete our approximate description of the physical system

$$S(\pm\Lambda,t) = 1, \quad Q(\pm\Lambda,t) = 0,$$
$$S(\pm\Lambda,0) = S_0(z), \quad Q(\pm\Lambda,0) = 0. \qquad (3.17)$$

3.4 Solution method

The time-dependent response of the shape of a liquid zone to axial residual accelerations was calculated and curves describing the tolerable acceleration as a function of the frequency of the axial acceleration were obtained for a variety of conditions. The dimensionless form of the residual acceleration was taken to be

$$g(t) = 1 + \frac{B_\omega}{B_0}\sin(\omega t), \qquad (3.18)$$

which was introduced in section 2. The initial shape was determined from computed static shapes corresponding to the static Bond number B_0 using a method similar to that employed by Meseguer [40].

3.4.1 Iteration procedure

In order to facilitate the solution of the system of eqs. (3.14)-(3.17) it is convenient to recast (3.15) and (3.16) in the form

$$\frac{\partial Q}{\partial t} + \frac{\partial}{\partial z}\left(\frac{Q^2}{S}\right) = -S\frac{\partial p^*}{\partial z} + CA(S)\frac{\partial^2}{\partial z^2}\left(\frac{Q}{S}\right) + CB(S)\frac{\partial}{\partial z}\left(\frac{Q}{S}\right), \qquad (3.19)$$

$$p^* = \frac{C}{4S + \left(\frac{\partial S}{\partial z}\right)^2}\left(2S\frac{\partial S}{\partial z}\frac{\partial^2}{\partial z^2}\left(\frac{Q}{S}\right)\right) + 4\left(4S + \left(\frac{\partial S}{\partial z}\right)^2\right)^{-\frac{3}{2}}\left(2S + \left(\frac{\partial S}{\partial z}\right)^2 - S\frac{\partial^2 S}{\partial z^2}\right) + Bz, \quad (3.20)$$

where

$$A(S) = S\,\frac{8S - \left(\frac{\partial S}{\partial z}\right)^2}{4S + \left(\frac{\partial S}{\partial z}\right)^2}, \quad (3.21)$$

and

$$B(S) = S\,\frac{12\left(\frac{\partial S}{\partial z}\right)^3 - 24S\frac{\partial S}{\partial z}\frac{\partial^2 S}{\partial z^2}}{\left(4S + \left(\frac{\partial S}{\partial z}\right)^2\right)^2}. \quad (3.22)$$

The solution scheme is based on a fully implicit time stepping procedure. However, since the position of the surface is unknown an iterative procedure is required to obtain solutions to the differential equations and the location of the surface at each time. The iterations proceed at each time step as follows:

(i) Guess the interface shape for the initial iterate.

(ii) The pressure p^* is calculated in the following way. All terms in (3.20) are calculated from the guessed values (or the previous iterate) except the leading viscous term. This is calculated from previous time steps using an Adams-Bashforth two-step approximation.

(iii) Q is then obtained upon solution of the momentum equation (3.19) and boundary conditions (3.17-3.18) using a Briley-McDonald implicit method [47-49].

(iv) The surface shape at the $m+1^{th}$ iterate is then obtained from a time-centered discretization of eq. (3.14).

(v) The surface shape is then compared with the initial guess (or the shape calculated at the m^{th} iterate). The procedure is repeated until the condition

$$\max\frac{|S_i^{m+1} - S_i^m|}{S_i^m} < 10^{-7} \quad (3.23)$$

is satisfied. Here a subscript 'i' denotes the value of s at the ith point, while the superscript denotes the iterative step.The above procedure is repeated at each time step.

The Briley-McDonald method used to solve (3.19) involves the evaluation of the non-linear advection term at the $n+1^{th}$ time step using

$$\left[\frac{\partial(Q^2/S)}{\partial z}\right]_i^{n+1} = \left[\frac{\partial(Q^2/S)}{\partial z}\right]_i^{n} + \Delta t\left[\frac{\partial}{\partial z}\left(\frac{\partial(Q^2/S)}{\partial t}\right)\right]_i^{n} + O\left((\Delta t)^2\right), \tag{3.24}$$

where the time derivative has been approximated using a forward difference and the space derivative with a centered difference. The time derivative on the right hand side of (3.24) is then approximated using a time-centered implicit scheme to increase the accuracy of the solution. The discretized form of (3.19) then becomes

$$\frac{Q_i^{n+1}-Q_i^{n}}{\Delta t} + \left[\frac{\partial(Q^2/S)}{\partial z}\right]_i^{n} + \frac{\Delta t}{2}\left[\frac{\partial}{\partial z}\left(\frac{\partial(Q^2/S)}{\partial t}\right)\right]_i^{n} = -\frac{1}{2}\left[\left(S\frac{\partial p^*}{\partial z}\right)_i^{n+1} + \left(S\frac{\partial p^*}{\partial z}\right)_i^{n}\right] +$$

$$\frac{C}{2}\left[A(S)\frac{\partial^2}{\partial z^2}\left(\frac{Q}{S}\right) + B(S)\frac{\partial}{\partial z}\left(\frac{Q}{S}\right)\right]_i^{n+1} + \frac{C}{2}\left[A(S)\frac{\partial^2}{\partial z^2}\left(\frac{Q}{S}\right) + B(S)\frac{\partial}{\partial z}\left(\frac{Q}{S}\right)\right]_i^{n}, \tag{3.25}$$

where a centered difference is used for spatial discretization. Eq. (3.25) is unconditionally stable and has second order accuracy with a truncation error of $O[(\Delta x)^2,(\Delta t)^2]$. The system of discretized equations and boundary conditions is solved using a Thomas algorithm [47].

3.4.2 Initial iterate

For this method of solution the choice of surface shape for the initial iterate at each time step affects the speed of convergence. For a poor choice the iteration may even fail to converge. To ensure that the initial iterate is reasonably close to the solution the following formula is employed

$$S_i^{n+1} = S_i^{n} + \Delta t\left(\frac{\partial S}{\partial t}\right)_i^{n} + \frac{1}{2}(\Delta t)^2\left(\frac{\partial^2 S}{\partial t^2}\right)_i^{n}. \tag{3.26}$$

For the computations presented here the number of iterations required was six or less whenever (3.23) was satisfied for the initial iterate.

3.4.3 Optimal searching scheme

In order to define the sensitivity limits for the liquid zone shape an optimal searching scheme was used to delineate the boundary between the regions in parameter space for which solutions either do or do not satisfy our sensitivity criterion. The scheme is described in the flow chart shown in Fig. 11. Eight to ten calculations were typically needed to obtain each point on the sensitivity curves.

3.4.4 Accuracy of the numerical scheme

An investigation into the accuracy of the results revealed that the number of timesteps per period of the disturbance should be at least 160. Increasing the number of steps to 400 per period did not, however, result in any siginificant change in our results even at high frequencies (see Table 4).

Table 4.

Δt	ω	Λ	B_0	g_T
0.00125	31.4	2.6	0.002	0.255
0.0005	31.4	2.6	0.002	0.256

The spatial accuracy also proved to be an important consideration. Results obtained using the MacDonald-Briley scheme described earlier required 97 spatial points. During the preliminary stages of this work other schemes used for the calculations, while performing adequately at low frequencies (less than 1 Hz) were found to fail at higher frequencies even when appropriate adjustments in time-step and space-step size were made.

3.5 Results

The sensitivity criteria chosen to characterize the response of the bridge represent two extremes. The first is the deviation of the the bridge radius by more than 10% from its equilibrium radius, the second is breakage of the bridge. The effects of viscosity, background steady acceleration (static Bond number, B_0) and slenderness (Λ) were examined and the results are presented below. Each point on these curves was obtained after running the calculation for times corresponding to more than 10 periods of the driving force. We note that for non-zero viscosity cases we found little difference between sensitivities calculated over 100 periods compared to those obtained

for 10 periods. This is not the case for inviscid bridges where considerably lower sensitivities may be obtained as the observation time is increased.

Figures 12 and 13 show the effect of viscosity on g_t for a frequency of 5 Hz at fixed Λ and B_o, for both sensitivity criteria. As expected the tolerance increases as the viscosity is increased. Notice, however, that for values of C less than 10^{-1} the increase in tolerance is slight even though the viscosity has been increased by two orders of magnitude. Only when C approaches 1 does the increase in tolerance become significant. Figures 14 and 15 further illustrate this point.

The value of the static Bond number has a more pronounced effect on sensitivity as seen in Figs. 16 and 17. This is limited, however to the lower frequency range. With increasing frequency the differences are less pronounced. This is particularly so for the shape change criterion. It is interesting to note the additional deviations from the general trend for the case of zone breakage between 10^{-1} and 1 Hz.

A small decrease in the slenderness Λ changes the magnitude of tolerable acceleration markedly when Λ is close to Λ_{max}. This is illustrated in Figs. 18 and 19. The change in tolerable acceleration magnitude becomes less significant for values of Λ less than 80% of the critical value.

Of most practical interest is the sensitivity of a given zone (i.e. Λ, B_o, and C fixed) as a function of the frequency of the disturbance. This is shown in Figs. 14-19. For both criteria the general trend is an increase in tolerable residual gravity with increasing frequency. For each situation there are, however, dramatic deviations from this trend. There is a particular frequency (corresponding to an eigenfrequency) at which the liquid zone is extremely sensitive in comparison to both higher and lower frequencies. The tolerable residual gravity level can be two orders of magnitude lower at this frequency. For the values of Λ and B_o considered these frequencies are found in the neighborhood of 10^{-1} Hz. Associated maximum tolerable residual gravity levels as low as 10^{-3} to 10^{-5} gal have been calculated. In addition, at frequencies higher than the most sensitive one there are less dramatic deviations from the general trend. The frequencies at which these deviations occur are the eigenfrequencies for the zone. As the frequency of the forcing function approaches an eigenfrequency the zone becomes more sensitive. As expected and predicted in [33], the lowest

tolerable acceleration occurs in conjunction with the smallest eigenfrequency.

Table 5. Tolerable acceleration (g_t) and associated eigenfrequencies (ω^*) for two of the cases computed for the shape change criterion.

$\Lambda = 3.024, B_0 = 0.002, C = 0$					
ω^*	0.21	4.0	11.0	20.5	33.5
g_t (m s^{-2})	6.0×10^{-6}	6.09×10^{-4}	1.88×10^{-3}	5.10×10^{-3}	5.06×10^{-3}
$\Lambda = 2.826, B_0 = 0.002, C = 0$					
ω^*	0.44	4.7	12.56	24	38.5
g_t (m s^{-2})	1.09×10^{-5}	7.79×10^{-4}	1.96×10^{-3}	4.76×10^{-3}	5.78×10^{-3}

Table 5 gives the eigenfrequencies and the associated maximum tolerable acceleration, g_t, for selected inviscid cases. For the inviscid zones, we found that whenever the higher eigenfrequency is close to an integer multiple of a lower eigenfrequency the sensitivity of the zone to disturbances with the higher frequency is increased. This noticeable increase in sensitivity is caused by non-linear interaction and excitation of the lower mode.

The spatial deformation of the liquid zone also varies as a function of the forcing frequency. Figures 20 and 21 illustrate the evolution of the zone shape as a function of time for selected cases. While higher forcing frequencies are associated with more nodes, the shape of the zone is complicated by the excitations of the fundamental mode and by non-linear interactions.

3.6 Discussion

The sensitivity of a cylindrical liquid zone to time-dependent axial residual accelerations has been investigated using a 1D numerical model. The results indicate that the zone is most sensitive to accelerations with frequencies close to or equal to the lowest natural frequency of the zone. For the purposes of this project it is most useful to assess the sensitivity of the zone in terms of predicted space-station and/or spacelab environments. We have seen that frequencies around the 0.1 Hz range appear to be the most sensitive. The low frequency

($< 10^{-2}$ Hz) acceleration environment predicted for the space station should not exceed levels of 10^{-5} gal [53]. Higher frequencies can be associated with acceleration magnitudes of up to 10^{-2} gal. In terms of these predicted levels, or those measured on past missions [54], the practical sensitivity range is restricted to disturbances with frequencies in the range 10^{-1} - 10 Hz.

It should be remembered that these results do not comprise a complete sensitivity analysis. Accelerations perpendicular to the zone axis have yet to be dealt with, and the effects of impulses have not been assessed. Future work along these lines, as well as extensions to include thermal effects is outlined in section 6.

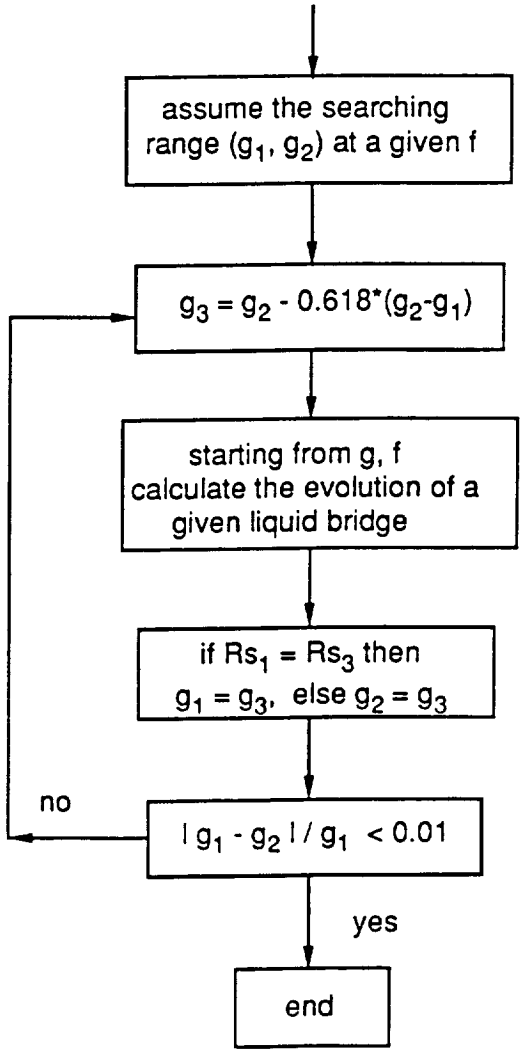

Fig. 11. Computational flow chart.

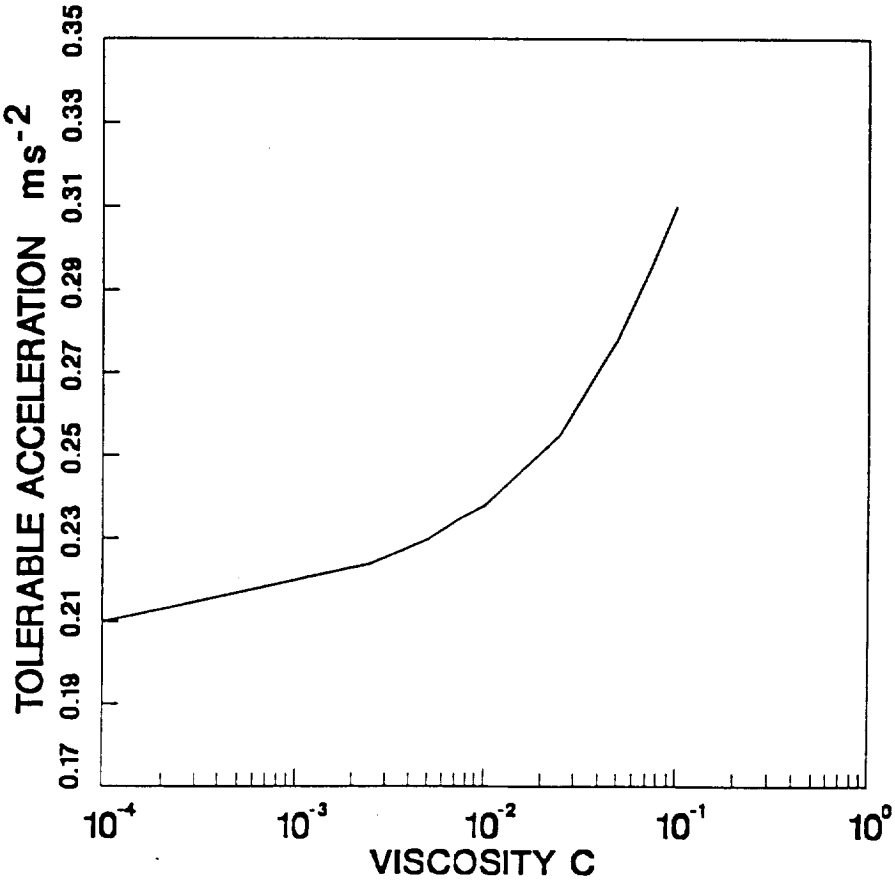

Fig. 12. Effect of viscosity on tolerable acceleration for breakage of the bridge at f =5Hz, L = 2.6 and Bo =0.002.

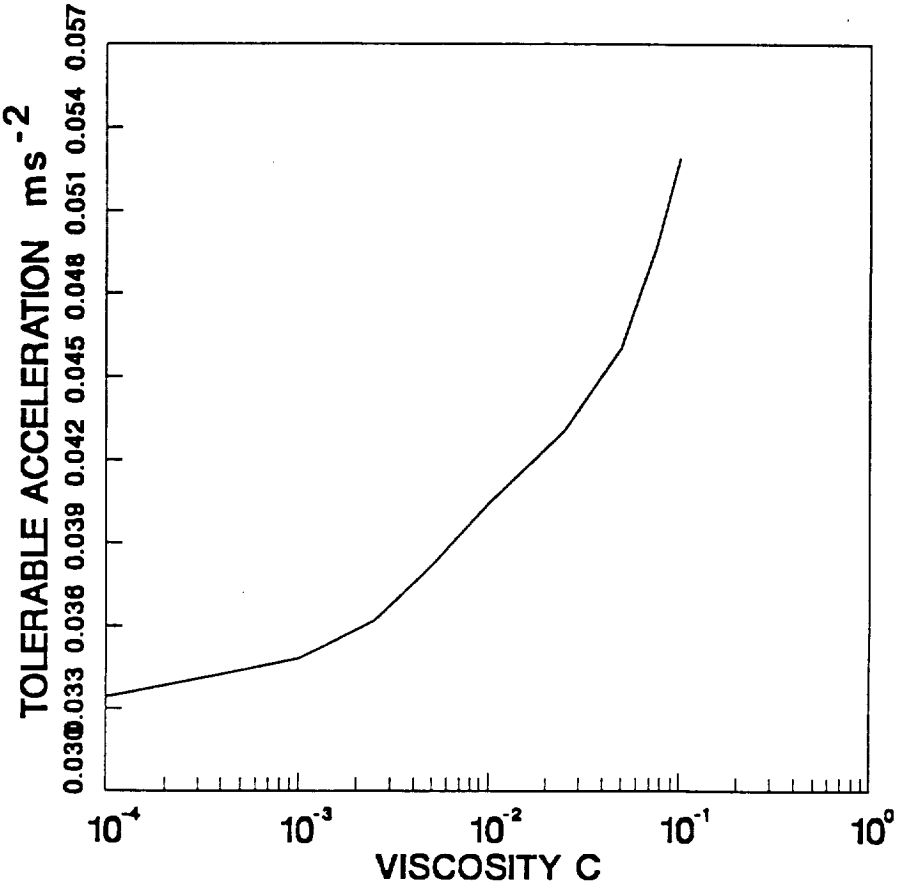

Fig. 13. Effect of viscosity on tolerable acceleration for the shape change criterion at f =5Hz, L=2.6 and Bo=0.002.

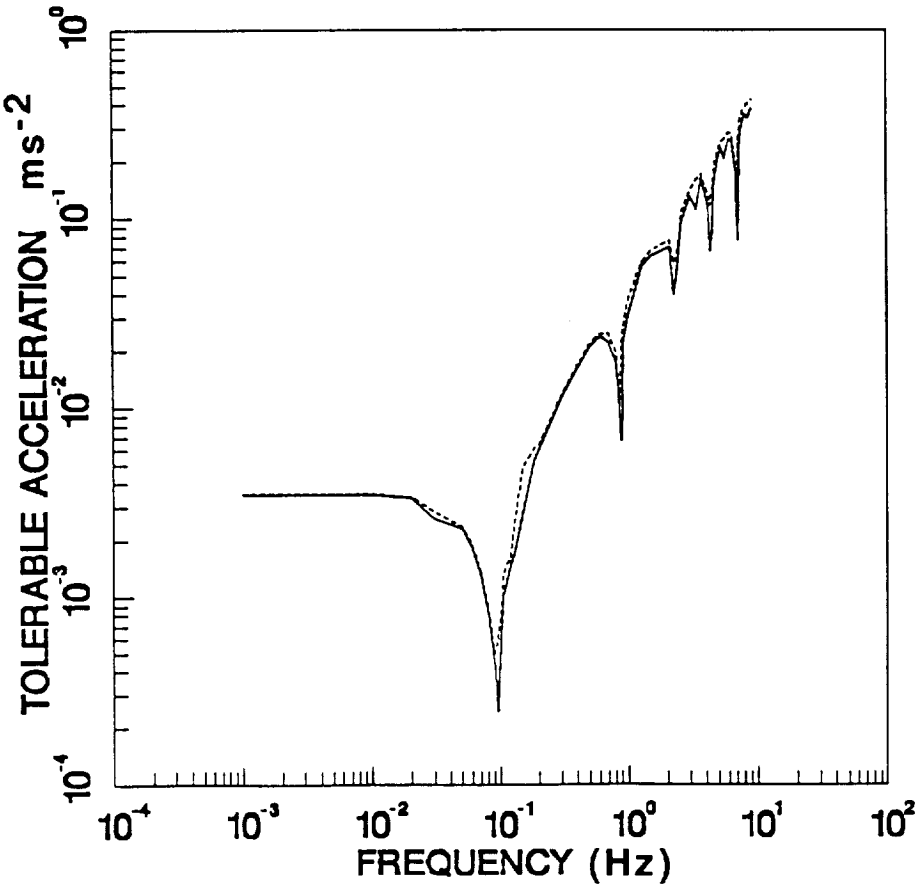

Fig. 14. Curves of tolerable acceleration versus frequency for breakage of the bridge at Bo=0.002 and L=2.6. The solid curve and the dashed curve are the results for C = 0.001 and 0.01, respectively.

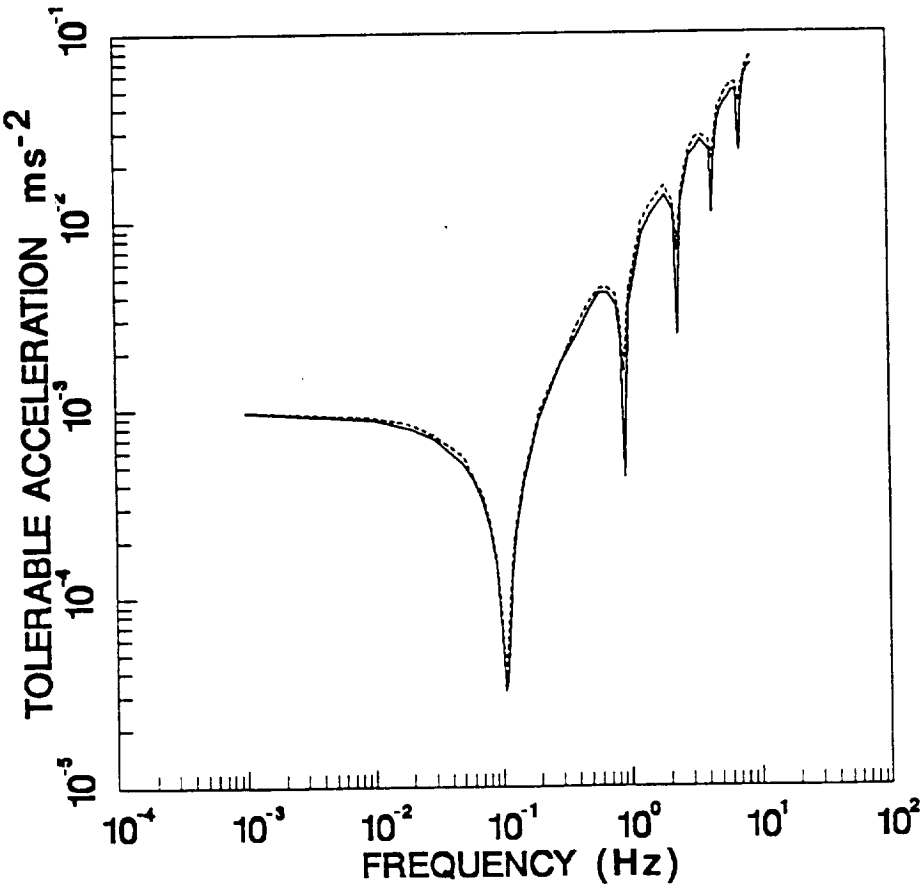

Fig. 15. Curves of tolerable acceleration versus frequency for shape change criterion at Bo=0.002 and L=2.6. The solid curve and the dashed curve are the results for C = 0.001 and 0.01, respectively.

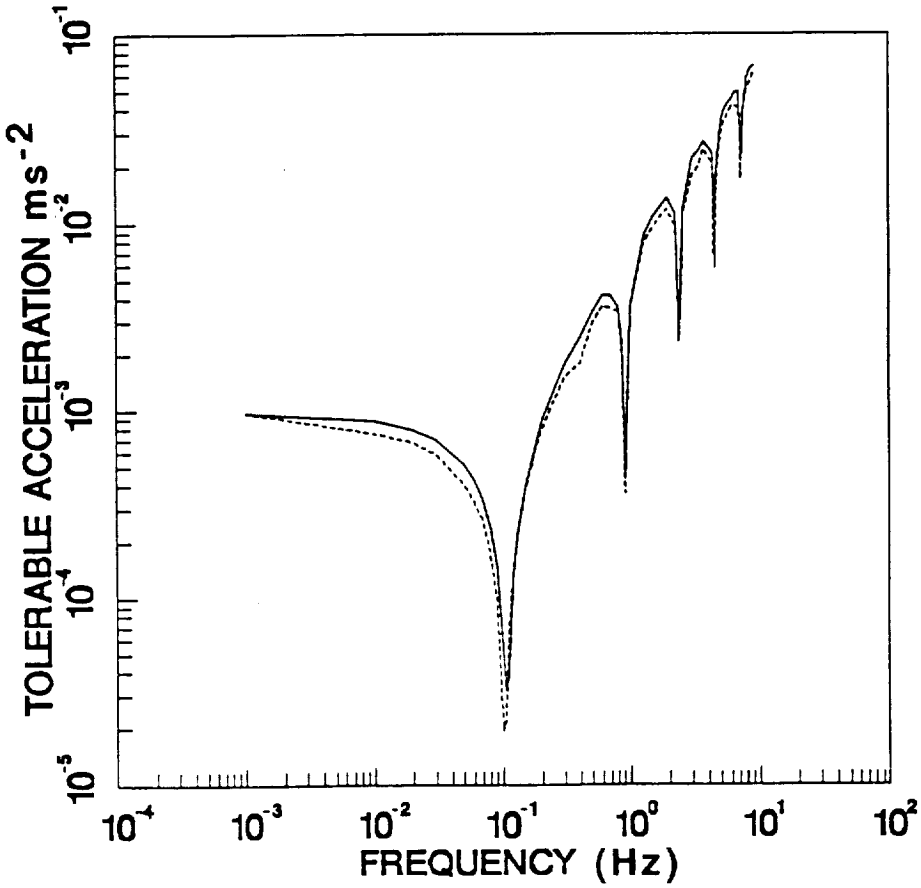

Fig. 16. Curves of tolerable acceleration versus frequency for shape change criterion at L= 2.6 and C =0.001. The solid curve and the dashed curve are the results for Bo=0.002 and 0.02, respectively.

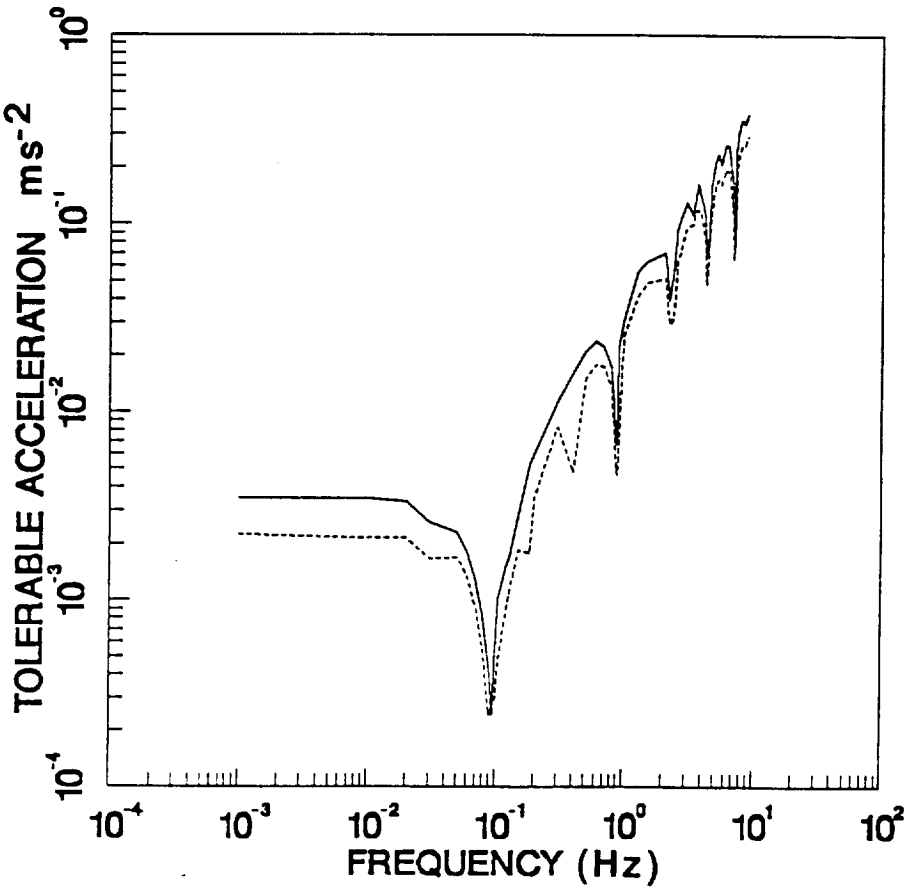

Fig. 17. Curves of tolerable acceleration versus frequency for breakage of the bridge at L =2.6 and C =0.001. The solid curve and the dashed curve are the results for Bo =0.002 and 0.02 , respectively.

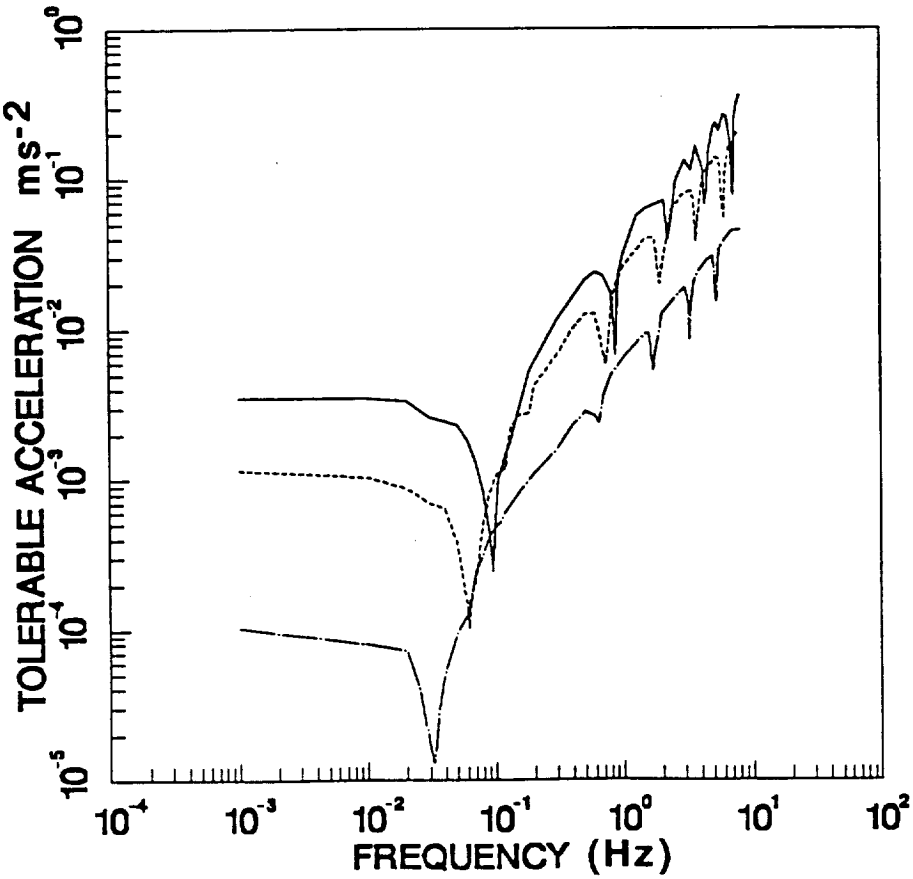

Fig. 18. Curves of tolerable acceleration versus frequency for breakage of the bridge at Bo = 0.002 and C = 0.001. The solid curve, the dotted curve and the dotted-dashed curve are the results for L=2.6, 2.826 and 3.024, respectively.

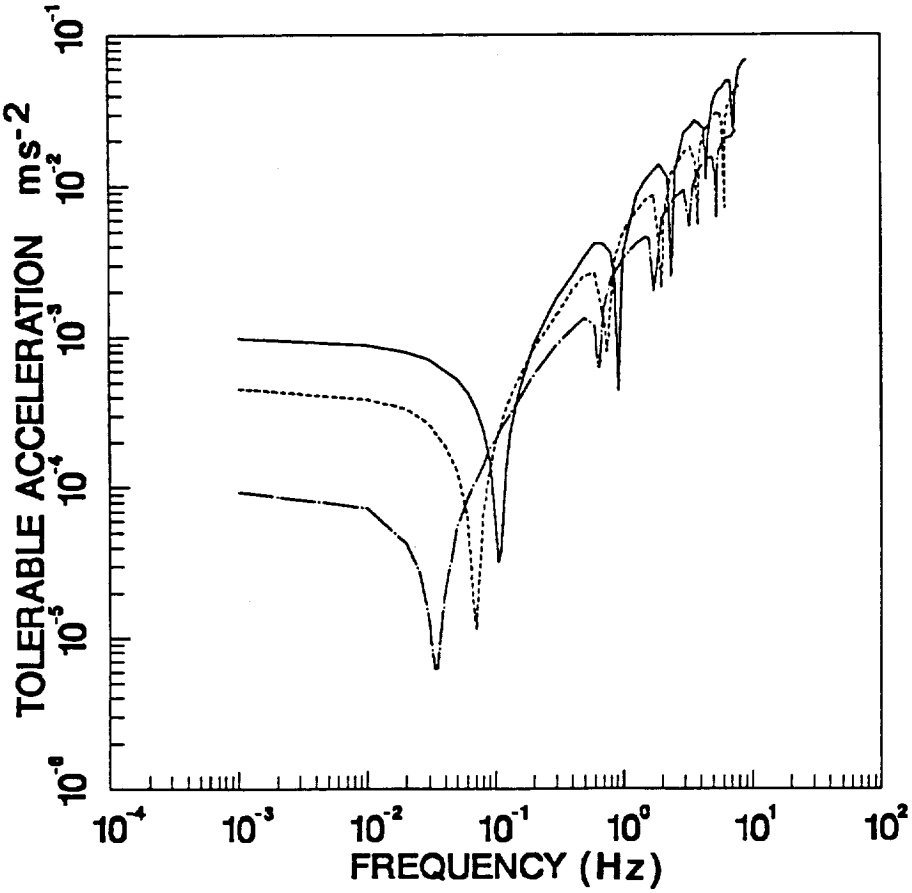

Fig. 19. Curves of tolerable acceleration versus frequency for the shape change criterion at Bo = 0.002 and C = 0.001. The solid curve, the dotted curve and the dotted-dashed curve are the results for L=2.6, 2.826 and 3.024, respectively.

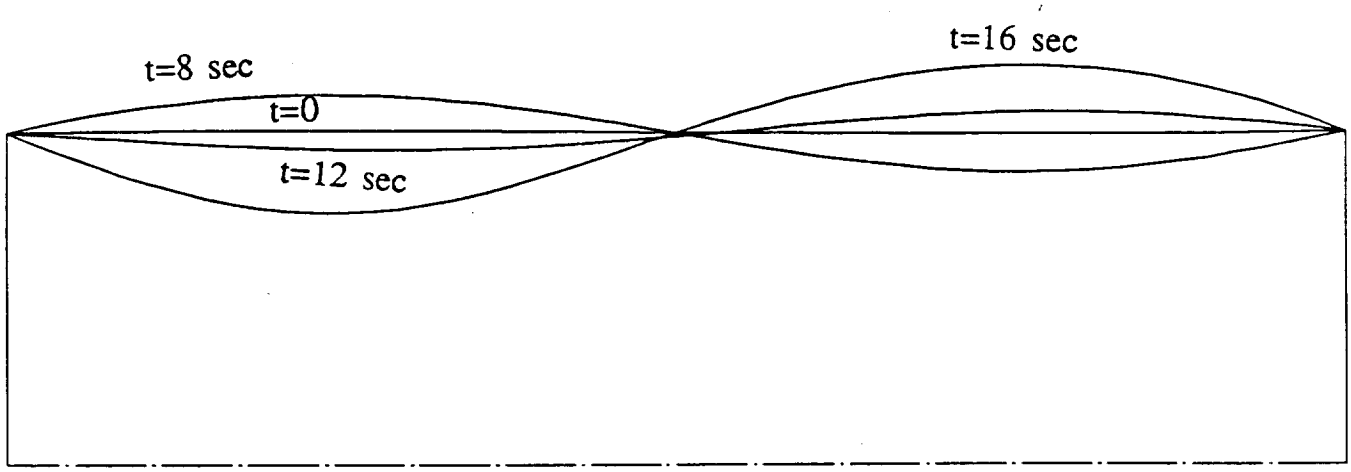

Fig. 20. Shape change as a function of time for a liquid zone with L =2.6, C =0.001 and g(t) =0.002(1+12 sin(0.377t)).

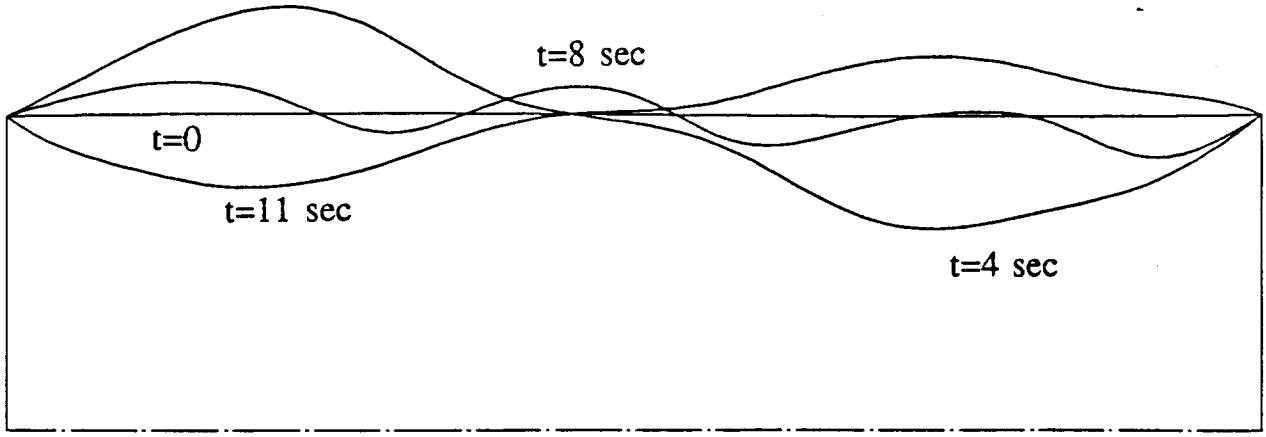

Fig. 21. Shape change as a function of time for a liquid zone with L = 2.6, C =0.001 and g(t) =0.002(1+916 sin(18.8t)).

4. Thermo-capillary convection

4.1 Introduction

Convection driven by surface tension involves the motion of a fluid in response to gradients in surface tension either at a free boundary of the fluid or at an interface between two fluids. The surface tension generally depends on scalar fields in the system such as the temperature field, concentration field or electric field. *Thermo*-capillary convection arises through the temperature dependence of the surface tension. In terms of the dynamics of a fluid system, surface tension and surface tension gradients play a role via the balance of forces at an interface.

When thermo-capillary convection occurs in an earth-based situation, it generally interacts with buoyancy-driven convection. A consequence of the high degree of non-linearity associated with such situations is that experimental isolation of the thermo-capillary effect is often impossible. As a result, studies of thermo-capillary flows have become one of the primary objectives of fluid physics experiments in microgravity.

At present our work is focused on thermo-capillary convection associated with a 2-D floating liquid zone. The objective is to study the effect of g-jitter on thermo-capillary flows for a range of dynamic Bond numbers $B^* = \rho g L^2/[\partial\gamma/\partial T]$ (here the denominator represents the change in surface tension with respect to temperature). At small (<< 1) but finite B^* , dimensionless analysis indicates that capillary forces should dominate [1]. However, the buoyancy forces may still affect the observed flow in the system, especially if these forces are oriented perpendicular to the basic temperature gradient in the system.

We are currently in the final stages of testing a method that has been developed by Dr. Adebiyi to solve the 2-D time dependent problem described below in section 4.2. The system of equations under consideration are described in section 4.3 and the solution scheme in 4.4. In section 4.5 our projected plans for the next six-month period are outlined.

4.2 Description of the model system

The physical system currently under examination involves a 2-D rectangular region (Fig. 22) which is bounded by two parallel walls and two free surfaces. The top and bottom walls are rigid and isothermal

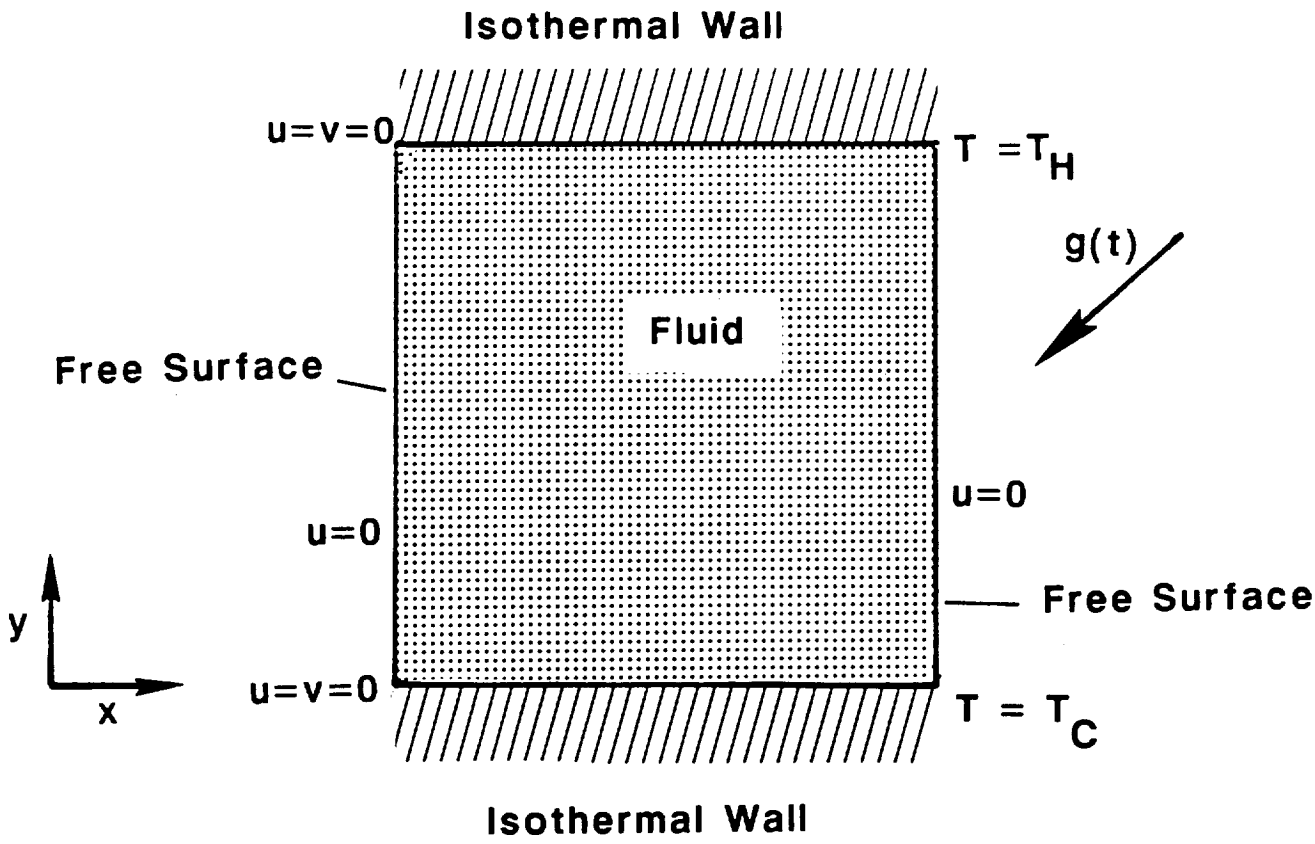

Fig. 22. The idealized thermo-capillary flow configuration.

with temperatures T_H and T_C respectively. The free surfaces are adiabatic (no perpendicular heat flux) and are constrained to be a straight line (zero crispation number approximation [50,51]). This retains the essential character of a free liquid surface while removing the numerical problems associated with a deformable one. The forces at the interface may be decomposed into components normal and tangent to it. Contributions to the force balance include the fluid pressure, the viscous forces and the capillary forces. For the normal component of force balance, the difference between the pressure and viscous forces on either side of the interface are proportional to the interface curvature multiplied by the surface tension γ. For the tangential force balance at the interface, the difference in the shear stress components is balanced by a gradient in surface tension. Such gradients will arise when there is a temperature gradient along the interface. The gradient in temperature produces a gradient in surface tension that induces shear stresses and, thus, fluid (thermo-capillary) motion. In our calculations the residual gravity vector is capable of taking any orientation with respect to the boundaries and can be time-dependent.

4.3 Governing equations and boundary conditions

Conservation of mass, momentum and energy within the incompressible fluid are described, respectively, by

$$\text{div } \tilde{\mathbf{v}} = 0, \tag{4.1}$$

and equations (2.9) and (2.10). The tangential force balance at the free fluid surfaces takes the form of (2.6). Thus, we assume implicitly that these surfaces are planar and non-deformable. The remaining boundary conditions are that the component of velocity normal to the free surfaces must vanish (consistent with our assumption that the surface remain planar) and that the velocity is zero at the two rigid walls (see Fig. 22).

4.3 Solution scheme

The problem is to be discretized in time and space.

4.3.1 Time discretization

(i) $$\frac{\partial u}{\partial t} \rightarrow \frac{u^{n+1} - u^n}{\Delta t}, \tag{4.2}$$

where u is the x-component of velocity.

(ii) The non-linear advection term is discretized in time using an Adams-Bashforth two-step explicit method [47] i.e.

$$u\frac{\partial u}{\partial x} \rightarrow \frac{3}{2}u^n \frac{\partial u^n}{\partial x} - \frac{1}{2}u^{n-1}\frac{\partial u^{n-1}}{\partial x}. \tag{4.3}$$

(iii) The viscous term is discretized using the Crank-Nicolson form [47]. This discretization takes the form

$$\nu\frac{\partial^2 u^{n+1}}{\partial x^2} = \frac{1}{2}\nu\frac{\partial^2 u^{n+1}}{\partial x^2} + \frac{1}{2}\nu\frac{\partial^2 u^n}{\partial x^2}. \tag{4.4}$$

(iv) The body force term is evaluated at the $n+1^{th}$ time step.

(v) The pressure term is dealt with as follows:

Rather than solve directly for the variables u,v,p, and T (here u and v are the two components of the velocity vector), two auxiliary variables p_1 and p_2 are introduced. These are equated with the pressure gradient in the x and y directions respectively, i.e.

$$\text{grad } p = (p_1, p_2). \tag{4.5}$$

The pressure at a location (x,y) is then related to p_1 and p_2 (which are expressed in Crank-Nicolson form) by simply integrating along some path from a fixed point $(\bar{x}, \bar{y})$ to (x,y):

$$p(x,y) = \int_{(\bar{x},\bar{y})}^{(x,y)} \left(p_1(\xi,\eta),p_2(\xi,\eta)\right)\cdot ds. \tag{4.6}$$

Thus, we have a system of six equations in the six unknowns (u,v,T,p_1,p_2,p).

The combination of the above representations comprises an Adams-Bashforth-Crank-Nicolson (ABCN) scheme. The time-discretized version of the above equations is now

$$(1- \alpha\Delta t\nabla^2)U^{n+1} = - \frac{1}{2}\Delta t p_1^{n+1} - \frac{1}{2}\Delta t p_1^{n} + H_u^n + F_u^{n,n-1} + G_u^{n+1}, \tag{4.7}$$

$$(1- \alpha\Delta t\nabla^2)V^{n+1} = - \frac{1}{2}\Delta t p_2^{n+1} - \frac{1}{2}\Delta t p_2^{n} + H_v^n + F_v^{n,n-1} + G_v^{n+1}, \tag{4.8}$$

$$(1- \beta\Delta t\nabla^2)\Theta^{n+1} = H_T^n + F_T^{n,n-1}, \tag{4.9}$$

$$\frac{\partial U^{n+1}}{\partial x} + \frac{\partial V^{n+1}}{\partial y} = 0, \tag{4.10}$$

$$p_1^k = \frac{\partial p^k}{\partial x}, \quad p_2^k = \frac{\partial p^k}{\partial y}, \quad k=n,n+1, \tag{4.11}$$

$$p^k(x,y) = \int_{\bar{x}}^{x} p_1^k(\xi,y)d\xi + \int_{\bar{y}}^{y} p_2^k(x,\xi)d\xi, \quad k=n,n+1, \tag{4.12}$$

and

$$U^{n+1} = u^{n+1} - u^n,\ V^{n+1} = v^{n+1} - v^n, \text{ and } \Theta^{n+1} = T^{n+1} - T^n, \tag{4.13}$$

where a subscript "u" or "v" refers to the appropriate u or v component of the momentum equation, H^n denotes the viscous term at the nth timestep, $F^{n,n-1}$ denotes the Adams-Bashforth expression for the non-linear term, while G^{n+1}, denotes the time-dependent body force term which includes the temperature T^{n+1}.

4.3.2 Spatial discretization using Tchebyshev polynomials

The system of equations in 4.3.1 can be written in operator form, i.e

$$\mathbf{Ax} = \mathbf{y}, \tag{4.14}$$

where

$$\mathbf{x} = \begin{pmatrix} U^{n+1} \\ V^{n+1} \\ \Theta^{n+1} \\ p_1^{n+1} \\ p_2^{n+1} \\ p^{n+1} \end{pmatrix}, \tag{4.15}$$

and $\mathbf{y}$ is vector containing the right hand sides of eqs. (4.7-4.13). This section gives an outline of the steps involved in constructing the matrix $\mathbf{A}$ (which contains the spatial derivatives owing to the Laplacian term) and the spatial approximation $\mathbf{x}$. It is expedient to outline these steps in terms of the spatial discretization of a function $w = w(x,t)$ which depends on one space variable only. The approach is readily extended to 2-D.

The function u and its derivatives will be approximated using Tchebyshev polynomials. The Tchebyshev polynomials are orthogonal polynomials defined on the interval [-1,1] and are given by $T_n(x) = \cos[n \arccos(x)]$ for each integer $n \geq 0$. We shall also make use of the fact that for $x=\cos\theta$, $T_n(x) = \cos(n\theta)$ for $\theta \in [0,\pi]$.

Now let w(x,t) be the function we wish to approximate. First we must carry out a transformation such that that the spatial domain of u lies on the interval [-1,1]. This will allow us to use Tchebyshev polynomials to approximate the spatial dependence of w.

Given

$$w_N(x,t) = \sum_{n=0}^{N} a_n(t) T_n(x),$$

we define collocation points x_k to be the set of points

$$\{x\} = \{x_k: x_k = \cos\frac{nk\pi}{N},\ k= 0,\ N\}.$$

Then w(x,t) can be expressed as

$$w(x,t) \approx w_N(x_k,t) = \sum_{n=0}^{N} a_n[e^{\frac{ink\pi}{N}} - e^{\frac{-ink\pi}{N}}]$$

$$= \sum_{n=-N}^{N} c_{|n|}a_{|n|}e^{\frac{-ink\pi}{N}}$$

$$\text{where } c_{|n|} = \begin{cases} 2 & |n| =0 \\ 1 & |n| >0 \end{cases}.$$

The coefficients a_n are determined from the Fourier transform of $w_k = w_N(x_k,t)$ and are :

$$\overline{c_n}\, a_n = \frac{2}{N}\sum_{k=0}^{N} \frac{1}{\overline{c_k}} u_k \cos(\frac{nk\pi}{N}),$$

$$= \frac{2}{N}\sum_{k=0}^{N} \frac{1}{\overline{c_k}} u_k T_k(x_n),$$

where

$$\overline{c_n} = \begin{cases} 2 & n= 0, N \\ 0 & n\neq 0,N \end{cases}.$$

The derivatives of w with respect to x can now be found directly or via the formula of Gottlieb and Orszag [52].

(i) Direct differentiation:

$$\frac{\partial w_N}{\partial x} = \sum_{n=0}^{N} a_n \frac{dT_n(x)}{dx}$$

$$T_n(x) = \cos n\theta,\ \theta = \arccos(x),$$

$$\frac{dT_n(x)}{dx} = -n\sin n\theta \frac{d\theta}{dx},$$

$$\frac{\partial w_N(x_k,t)}{\partial x} = \sum_{n=0}^{N} a_n(t)\frac{n\sin n\theta_k}{\sin\theta_k}$$

$$= \sum_{n=0}^{N}\sum_{i=0}^{N} \left(\frac{2}{N\overline{c}_n\overline{c}_i} T_i(x_n) \frac{n\sin\theta_k}{\sin\theta_k} u_i \right)$$

so for $w_k = w_N(x_k,t)$

$$\frac{\partial w_k}{\partial x} = D_x w_k = \sum_{n=0}^{N} L_{ki} w_i,$$

$$L_{ki} = \sum_{n=0}^{N} \frac{2}{N \bar{c}_n \bar{c}_i} T_i(x_n) \frac{n \sin\theta_k}{\sin\theta_k},$$

where L_{ki} is the first derivative operator. In this manner, with a Tchebyshev series approximation in both the x and y directions, the spatial derivatives can be calculated for our 2-D problem. The second derivative operator which is contained in **A** can be obtained from the matrix product of L with itself or from the formulae in [52].

The components of **y** (which include derivative terms at the previous (n^{th}) and $(n-1)^{th}$ time step such as H^n and $F^{n,n-1}$) are obtained from recurrence formulae for the derivatives expressed in terms of the a_n calculated at the previous timestep. Recall that we have not yet mentioned the boundary conditions which must be incorporated in equation (4.14) must now be modified to include the boundary conditions. This is done by replacing the components of **Ax** = **y** at boundary locations with the appropriate terms corresponding to the discretized boundary conditions.

The boundary conditions will take the form

$$U^{n+1} = V^{n+1} = 0 \text{ at the walls, } U^{n+1} = 0 \text{ at the free surface,} \qquad (4.15)$$

$$\Theta^{n+1} = 0 \text{ at the walls,} \qquad (4.16)$$

and

$$-\mu \frac{\partial U^{n+1}}{\partial x} = \gamma \frac{\partial \Theta^{n+1}}{\partial y}, \text{ at the free surface.} \qquad (4.17)$$

4.3.3 Implementation

Having completed the temporal and spatial discretization, it now remains to outline the procedure by which a solution is obtained at each time step. The system of equations (4.7-4.13) together with the boundary conditions (4.15-4.17) which are written in the form (4.14) are now inverted to obtain **x**. For this method we may define a

residual as

$$\varepsilon = |\text{div } \mathbf{v}|, \tag{4.18}$$

and iterate until ε is sufficiently small. Having satisfied (4.18), time is advanced and the procedure repeated. This scheme differs from the one described in our first semi-annual report in only three ways. Firstly, it deals with the pressure by introducing auxiliary dependent variables corresponding to the components of the pressure gradient and computing the pressure via integrals. The pressure is solved on a separate grid which enables explicit computation of the boundary values of the pressure to be avoided. Secondly, the scheme does not employ the alternating direction implicit method (ADI). The third difference is that the method of artificial compressibility is not employed.

4.4 Progress and planned work

The scheme described in the previous section is currently being tested. We expect to be able to present preliminary results for the thermo-capillary problem in the upcoming Alabama Materials Science Meeting in September 1989 (see appendix B). During the next six month period we plan to apply the method described above to the problem outlined in sections 4.1 and 4.2, and to compare it with results obtained using the scheme described in the first semi-annual report, and with the results of calculations undertaken at MSFC.

The calculations will take the form of a parametric study of the response of the "two surface" model depicted in Fig. 22, to single component periodic disturbances and impulses, and will later be extended to include an examination of the response to multicomponent disturbances (both periodic and non-periodic).

5. Interaction with NASA personnel

Interaction with NASA personnel during the first semi-annual period has involved an introductory meeting with J. Lubomski, C. Grodzinsky (NASA/LeRc), C. Schafer and Cheryl Winter (MSFC) at UAH. In addition, the P.I. gave a presentation at the Vibration Isolation Technology Workshop at Lewis Research Center, Cleveland, 9/28-29/88. There have also been several informal discussions with Cheryl

Winter (MSFC) and Dr. Ramachandran (USRA/MSFC).

One outcome of the V.I.T. Workshop was contact with personnel involved in analysis of Space Station Structure (J. Sullivan [Wyle/RestonVa.]). Mr. Sullivan has provided us with preliminary data concerning predicted dynamics. This should provide a basis for constructing more realistic g-jitter functions as input for our numerical models.

6. Summary and discussion/Work planned for the second year

The work undertaken to date includes a survey of published work relevant to the transport of heat and mass in fluids subject to vibration, a detailed analysis of the sensitivity of liquid zones to time-dependent axial acceleration, and the development of a 2-D numerical model of mixed buoyancy-driven thermo-capillary convection. It appears that for the latter the most sensitive frequency ranges (in terms of the expected space station acceleration environment) appear to be in the 0.1-10 Hz range.

Two manuscripts intended for publication are close to completion and are based on work undertaken during the first year of this study. One is based on our liquid zone calculations and describes our work to date on liquid zone sensitivity. The other is a review of literature related to sensitivity of experiments to residual acceleration and the effects of oscillating body forces and vibration on heat and mass transfer in fluid systems. In addition we plan to participate in the upcoming 3rd Alabama Materials Research Conference, September 20-21, 1989, at the University of Alabama in Huntsville. Three abstracts are included in appendix B.

Extensions of the first year's work to be carried out during the second and third years will include an examination of the effects of viscosity and the effect of accelerations oriented perpendicular to the fluid surface for the liquid zone sensitivity analysis. The scope of work involving thermo-capillary flow, and the time frame involved, dictates that the numerical modelling will be in some sense "generic" (as discussed in the original proposal). The effect of transient disturbances, multiple frequency vibrations, and magnitude and orientation of the disturbances will be examined. In addition, residual acceleration profiles which simulate recorded disturbances aboard the Orbiter will be examined.

7. References

[1] S. Ostrach, Ann. Rev. Fluid Mech. 14 (1982) 313.

[2] R. Monti, J.J. Favier and D. Langbein, in Fluid Sciences and Materials Science in Space, A European Perspective, Ed. H. U. Walter (Springer, Berlin 1987) p. 637.

[3] D. Langbein, ESA Contract Report, BF-R-66.525, April 1987.

[4] L. Napolitano, Ann. N.Y. Acad. Sci. (1983) 278.

[5] M. D. Radcliffe, M. C. Drake, G. Zvan, W. W. Fowlis, J. I. D. Alexander, G. D. Roberts, J. K. Sutter and E. Bergman, in Proceedings of the American Chemical Society Meeting, New Orleans 1987.

[6] J. I. D. Alexander, J. Ouazzani and F. Rosenberger, Analysis of Low Gravity Tolerance of Model experiments for Space Station: Bridgman Technique 1st Semi-annual Progress Report NASA Grant NAG8-684 April 14th 1988.

[7] J. I. D. Alexander, J. Ouazzani and F. Rosenberger, *Analysis of the low gravity tolerance of crystal growth experiments employing the Bridgman-Stockbarger technique.*
a) *I: Steady and impulse accelerations*, J. Crystal Growth to appear 1989.
b) *II: Transient and periodic accelerations*, in preparation 1989.

[8] A. Rouzaud, D. Camel and J. J. Favier, J. Crystal Growth 73 (1985) 149.

[9] D. Camel and J.J. Favier, J. de Physique 47 (1986) 1001.

[10] C. J. Chang and R. A. Brown, J. Crystal Growth 63 (1983) 353.

[11] S. Ostrach and A. Pradhan, AIAA Journal 16 (1978) 419.

[12] L. G. Napolitano, R. Monti, G. Russo and C. Golia, Proc. 6th European Symposium Materials Sciences in Microgravity Conditions, Bordeaux, France (ESA SP-256 1987) p. 191.

[13] D. Schwabe and A. Scharmann, Proc. 5th European Symposium Materials Sciences in Microgravity Conditions, Schloβ Elmau FRG (ESA SP-222 1984) p. 81.

[14] L. G. Napolitano, R. Monti and G. Russo, *ibid.* p. 15.

[15] Ch-H. Chun, Proc. 5th European Symposium Materials Sciences under Microgravity, Schloss Elmau, (ESA SP-222 1984) p. 271.

[16] D. Langbein and U. Roth, Proc. 6th European Symposium Materials Sciences in Microgravity Conditions, Bordeaux, France (ESA SP-256 1987) p. 183.

[17] S. Ostrach and Y. Kamotani, NASA Technical Memorandum 4069 Microgravity science and applications flight program Vol. 2. (1988) 695.

[18] Y. Kamotani, S. Ostrach and M. Vargas, J. Crystal Growth 66 (1984) 83.

[19] E. L. Koschmieder and M. Biggerstaff, J. Fluid Mech. 167 (1986) 49.

[20] E. N. Ferm and D. J. Wollkind, J. Non-Equilib. Thermodyn. 7 (1982) 169.

[21] R. W. Zeren and W. C. Reynolds, J. Fluid Mech. 53 (1972) 305.

[22] A. Cröll, W. Mueller and R. Nitsche, Proc. 6th European Symposium Materials Sciences in Microgravity Conditions, Bordeaux, France (ESA SP-2561987) p. 87.

[23] S. P. Murphy, J. J. Hendrick, M. J. Martin, R. W. Grant and M. D. Lind, Mat. Res. Soc. Symp. Proc. 87 (1987) 139.

[24] M. D. Lind, AIAA-Paper 87-0618 (25th Aerospace Sciences Meeting, Reno, January 19-27, 1987).

[25] M. D. Lind, J. J. Hendrick and M. J. Martin, in Low gravity sciences ed. J. Koster, Vol 67 science and technology series (Univelt, San Diego, 1987) 149.

[26] I. Martinez, Proc. 5th European Symposium on Materials Sciences under Microgravity, Schloss Elmau FRG, ESA SP-222 (1984), p. 31.

[27] J. Haynes, *ibid*. p. 43.

[28] I. Martinez, Proc. 6th European Symposium on Materials Sciences in Microgravity Conditions, Bordeaux, France (ESA SP-256 1987) p. 235.

[29] J. F. Padday, *ibid*. p. 251.

[30] R. F. Sekerka and S.R. Coriell, Proc. 3rd European Symposium on Materials Science in Space, Grenoble France, (ESA-SP-256 1979) p. 55.

[31] I. Martinez, J. M. Haynes and D. Langbein, in Fluid Sciences and Materials Science in Space, A European Perspective, Ed. H. U. Walter (Springer, Berlin 1987) p. 53.

[32] S. R. Coriell, S. C. Hardy and M. R. Cordes, J. Colloid and Interface Sci. 60 (1977) 126.

[33] D. Langbein, Proc. 6th European Symposium on Materials Sciences in Microgravity Conditions, Bordeaux, France (ESA SP-256 1987) p. 221.

[34] Y. C. Zhang, to be published 1989, (see also section 3 of this report.)

[35] C.E. Chang and W.R. Wilcox, J. Crystal Growth 28 (1975) 8.

[36] W. Heywang, Zeitschrift für Naturforsch. 11a (1956) 238.

[37] S. R. Coriell, S. C. Hardy and M. R. Cordes, J. Crystal Growth 42 (1977) 466.

[38] J. Duranceau and R. A. Brown, J. Crystal Growth 75 (1986) 367.

[39] H. C. Lee, I.B.M. J. Res. Dev. 18 (1974) 364.

[30] J. Meseguer, J. Fluid Mech. 130 (1983) 123.

[41] D. Rivas and J. Meseguer, J. Fluid Mech. 138 (1984) 417.

[42] J. Meseguer and A. Sanz, J. Fluid Mech. 153 (1985) 83.

[43] A. Sanz, J. Fluid Mech. 156 (1985) 101.

[44] J. Meseguer, J. Crystal Growth 73 (1985) 599.

[45] J. Meseguer, A. Sanz and J. Lopez, J. Crystal Growth 78 (1986) 325.

[46] J. Meseguer, Appl. Microgravity Tech. 1 (1988) 136.

[47] R. Peyret and T. D. Taylor, Computational Methods for Fluid Flow (Springer, New York, 1983).

[48] W. R. Briley and H. McDonald, An Implicit Numerical Method for the Multidimensional Nonstaionary Navier-Stokes Equations.

United Aircraft Research Laboratory Rept. M911363-6, (1973).

[49] W. R. Briley and H. McDonald, J. Comput. Physics 24 (1977) 372.

[50] J. R. Pearson, J. Fluid Mech. 4 (1958) 489.

[51] S. H. Davis, Ann. Rev. Fluid Mech. 19 (1987) 403.

[52] D. Gottlieb and S. A. Orszag, Numerical Analysis of Spectral Methods, (SIAM, Philadlephia, 1977).

[53] J. Sullivan, Grumman Space Station Freedom Program Support Division, Reston Virginia, personal communication.

54] H. Hamacher, R. Jilg, U. Mehrbold, Proc. 6th European Symposium Materials Sciences in Microgravity Conditions, Bordeaux, France (ESA SP-256 1987).

8. Appendices

8.1 Appendix A

Task 1: Order of magnitude analyses

This task involves preliminary estimates of sensitivity levels using order of magnitude estimates and analytical solutions for the classes of experiments discussed in the original proposal. Order of magnitude estimates pertaining to tasks 2, and 4 have been completed and a journal publication describing these results along with a review of past work pertinent to analyses of experiment sensitivity to time-dependent acceleration is close to completion.

Task 2 : Thermo-capillary convection - two dimensional

This aspect of the project is focused on thermo-capillary convection associated with a 2-D floating liquid zone. The objective is to study the effect of g-jitter on thermo-capillary flows for a range of dynamic Bond numbers $Bd = \rho g L^2/[\partial\sigma/\partial T]$ (here the denominator represents the change in surface tension with respect to temperature). In order to solve the full non-linear equations governing the behavior of the system, a pseudo-spectral collocation method is being adapted to discretize the problem in space and time.

This task was originally described as "Thermo-capillary - axisymmetric" and was scheduled to start after six months. Preliminary results have been obtained, but work has been slowed recently due to personnel changes. The scope of this work, and the time frame involved, dictates that the numerical modelling will be in some sense "generic" (as discussed in the original proposal). The effect of transient disturbances, multiple frequency vibrations, and magnitude and orientation of the disturbances will be examined. In addition, residual acceleration profiles which simulate recorded disturbances aboard the Orbiter will be examined.

Task 3: Thermo-capillary convection - three dimensional and axisymmetric

This task has been redefined to include an examination of axisymmetric as well as fully three-dimensional conditions. The work described in tasks 2 and 1 will be used to determine the cases to be computed. Preliminary work is planned to begin in the second half of the third year. This task will concentrate on the effects of variable magnitude and orientation of time-dependent residual accelerations. Of particular interest is the extent to which residual accelerations can

result in non-axisymmetric flow conditions, for cases which 2-D analyses indicate a marked sensitivity to residual accelerations a three-dimensional analysis is justified. Owing to computational time limitations, full three-dimensional calculations can only be made for a limited number of cases.

Task 4: Liquid Bridge/ Floating-Zone Sensitivity

This task involves numerical modelling of the response of float zone shapes to variable magnitude and orientation of time-dependent residual accelerations. Although it was originally proposed to examine only the linear response of the bridge, we have been able to formulate a model of the non-linear response. Work was started in October 1989 (3 months earlier than originally scheduled). Extensions of the first years work to be carried out in the second and third years will include an examination of the effects of viscosity and the effect of accelerations oriented perpendicular to the fluid surface.

8.2 Appendix B. Abstracts of presentations to be made at the Alabama Materials Research Conference, University of Alabama in Huntsville, September 20th & 21st,1989.

SENSITIVITY OF LIQUID BRIDGE AND FLOATING ZONE SHAPES SUBJECT TO AXIAL VIBRATIONS

Y. Q. Zhang and J. Iwan D. Alexander

Center for Microgravity and Materials Research
University of Alabama In Huntsville
Huntsville, Alabama 35899
Tel. (205) 895 6248

It has become evident that both the float zone crystal growth method and isothermal liquid bridges may be very sensitive to the residual acceleration environment of a spacecraft. Using a slender-body approximation, the problem of determining the axisymmetric response of the shape of the free surface of a cylindrical liquid column bounded by two solid regions is modelled by a 1-D system of equations. Although the reduction in dimensionality simplifies the equations, they are still highly non-linear. The results can be summarized as follows:

a) The sensitivity of the zone shape depends on the static Bond number, aspect ratio and viscosity as well as the amplitude and frequency of the disturbance.

b) The general trend is an increase in tolerable residual gravity with increasing frequency.

c) For each situation there are, however, dramatic deviations from this trend. There is a particular frequency at which the sensitivity is extreme in comparison to other frequencies. The tolerable residual gravity level for this frequency can be two orders of magnitude lower than for other frequncies. In addition, at other frequencies there are less dramatic deviations from the general trend. To date the most sensitive frequencies have been found in the 10^{-1}-1 Hz range. Associated maximum tolerable residual gravity levels as low as 10^{-5} g have been calculated.

EXPERIMENTS IN LOW GRAVITY AND THEIR SENSITIVITY TO RESIDUAL ACCELERATION: A REVIEW

J. Iwan D. Alexander

Center for Microgravity and Materials Research
University of Alabama In Huntsville
Huntsville, Alabama 35899
Tel. (205) 895 6248

The sensitivity of a given experiment or process to the microgravity environment will depend on one or more of the following factors:

a) geometry

b) magnitude and direction of accelerations

c) boundary conditions (eg. insulated or conducting walls, solute sources and sinks)

d) physical properties of the participating materials (viscosity, thermal and solute diffusivities)

Examples of experiments (past and future) that take advantage of the low gravity environment include critical point studies, crystal growth, solidification of metal alloys and model alloy systems, and diffusion experiments. However, these experiments involve density gradients in the nutrient fluid phase and, thus, are inherently sensitive to the effects of buoyancy-driven fluid motion.

The analysis of the sensitivity of any proposed flight experiment is necessary for a variety of reasons. These include the need to optimize the use of the limited time available for flight experiments, the interpretation of experimental results and the determination of tolerable acceleration levels to be used in planning space laboratory facilities. This paper reviews work related to the determination of the sensitivity of experiments to externally imposed steady and time-dependent accelerations associated with microgravity environments. The context in which the results of such analyses should be viewed is discussed, and the viability of using more sophisticated models as part of the general approach to space experiment development is also addressed.

THERMO-CAPILLARY CONVECTION IN A LOW-GRAVITY ENVIRONMENT

Adebimpe Adebiyi and J. Iwan D. Alexander

Department of Mathematics and
Center for Microgravity and Materials Research
University of Alabama In Huntsville
Huntsville, Alabama 35899
Tel. (205) 895 6248

We present results of 2-D numerical models of convection driven by both bouyancy and surface tension. The bouyancy source is taken to represent conditions asscociated with the (time dependent) low effective gravity environment of a spacecraft. Convection driven by surface tension is caused by gradients in surface tension either at a free boundary of a fluid or at an interface between two fluids. The surface tension gradients arise due to gradients in surface temperature or composition.

Thermo-capillary convection occurs in a variety of crystal growth systems (eg. the float-zone technique) for which part of the melt surface is not in contact with a solid. As a result, the last decade has seen a variety of approaches directed at gaining a better understanding of surface-tension driven flow and its importance in crystal growth systems. When thermo-capillary convection occurs in an earth-based situation, it generally interacts with buoyancy-driven convection and isolation of the thermo-capillary effect is often impossible. As a result, the microgravity environment provides attractive conditions for materials scientists and fluid physicists to study thermo-capillary flows. Our numerical models are intended to illustrate the consequences of undertaking such experiments in space and to identify trends which will allow the maximum benefit to be derived from use of space laboratories.